conference Mechanics in Aviation XVI, 26-29 May 2014, Kazimierz Dolny

"What do dynamical calculations of birch trunk deformation & breaking, and of the flight of the detached wing fragment tell us about the catastrophe of flight PLF 101 in Smolensk"

Paweł Artymowicz

University of Toronto

TOPICS

- Where and when was the wintip of TU-154M detached from the aircraft?
- How was it moving and how far did it fly?

- Where did the fatal half-roll of flight PLF 101 begin?

- What was happening with the birch tree during the collision? Did the wingtip separate from the aircraft or cut the this birch and remain attached to the rest of the wing?

Incorrect calculations of Dr. Binienda et al. (2012)

Hypothesis of a 10-12 meter flight with sudden, unexplained braking in mid-air.

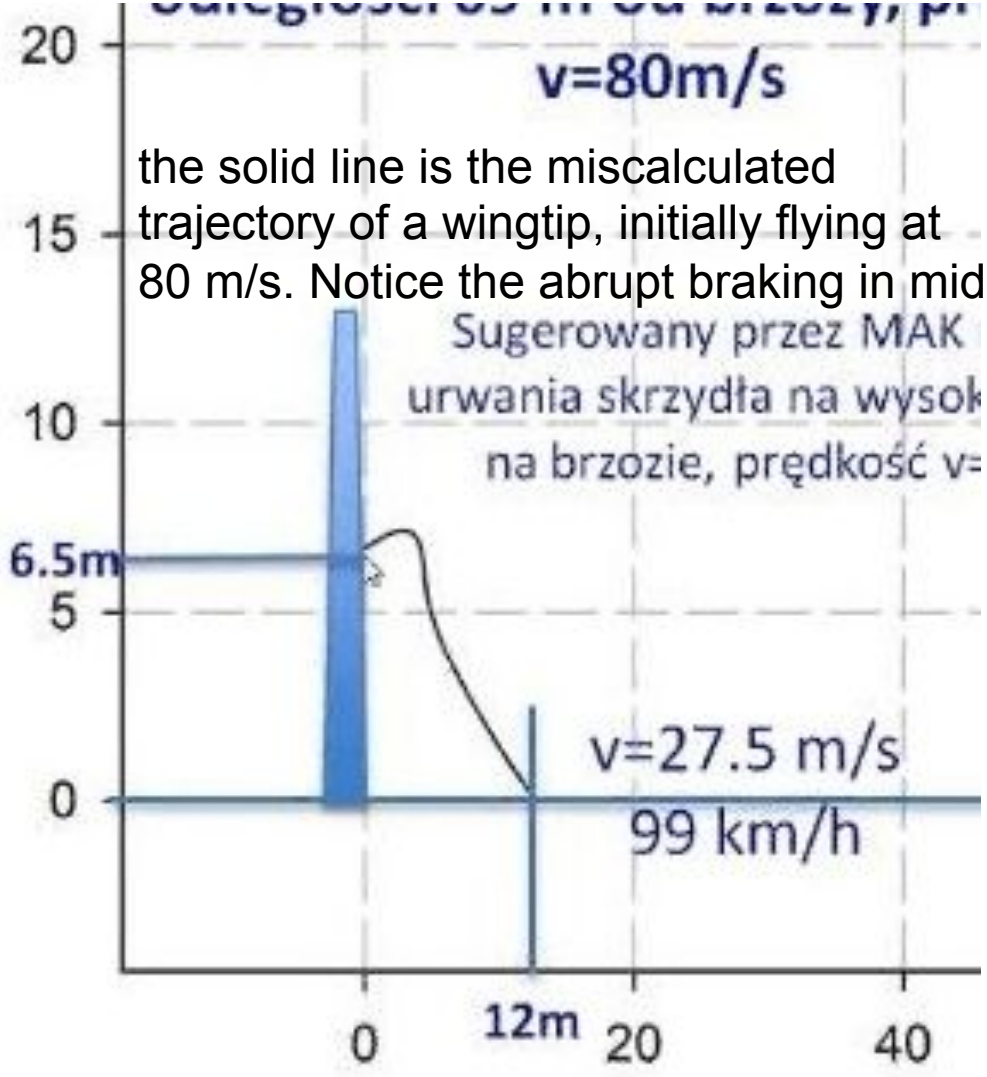

Such a scenario requires: either a deceleration in air reaching the value of 60 g, i.e. coefficient of drag Cd ~ 20-30, or air density 20-30 times higher than actual, the mass of the wing too low 20x, or (quite likely!) the Reynolds number Re in model orders of magnitude too low as a consequence of low resolution or otherwise wrong numerical calculations).

Pick your favorite reason – Binienda's calculations are wrong in any case.

Binienda (2012) did FEM analysis of wing-tree collision. He did not know either the true thicknesses of aluminum alloy sheets (D16) or even the correct range in which they should lie. His models had metal 5-12 mm thick, which is 3-4 times too high. We now know the dimensions directly from Tupolev design bureau. Every engineer should be able to estimate the required thickness for transport aircraft to +-20% accuracy.

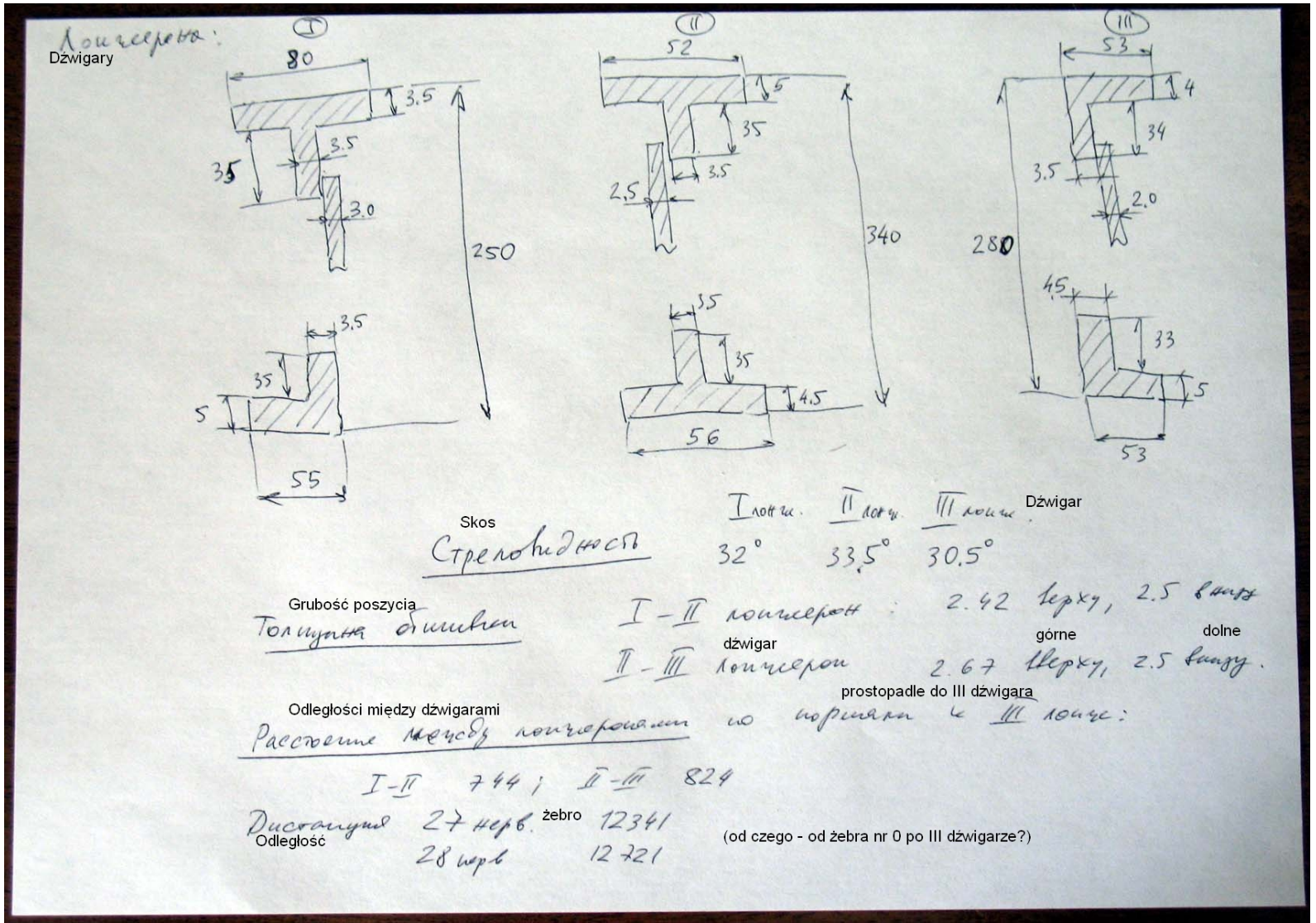

My results for flightpath of a wingtip in 2012

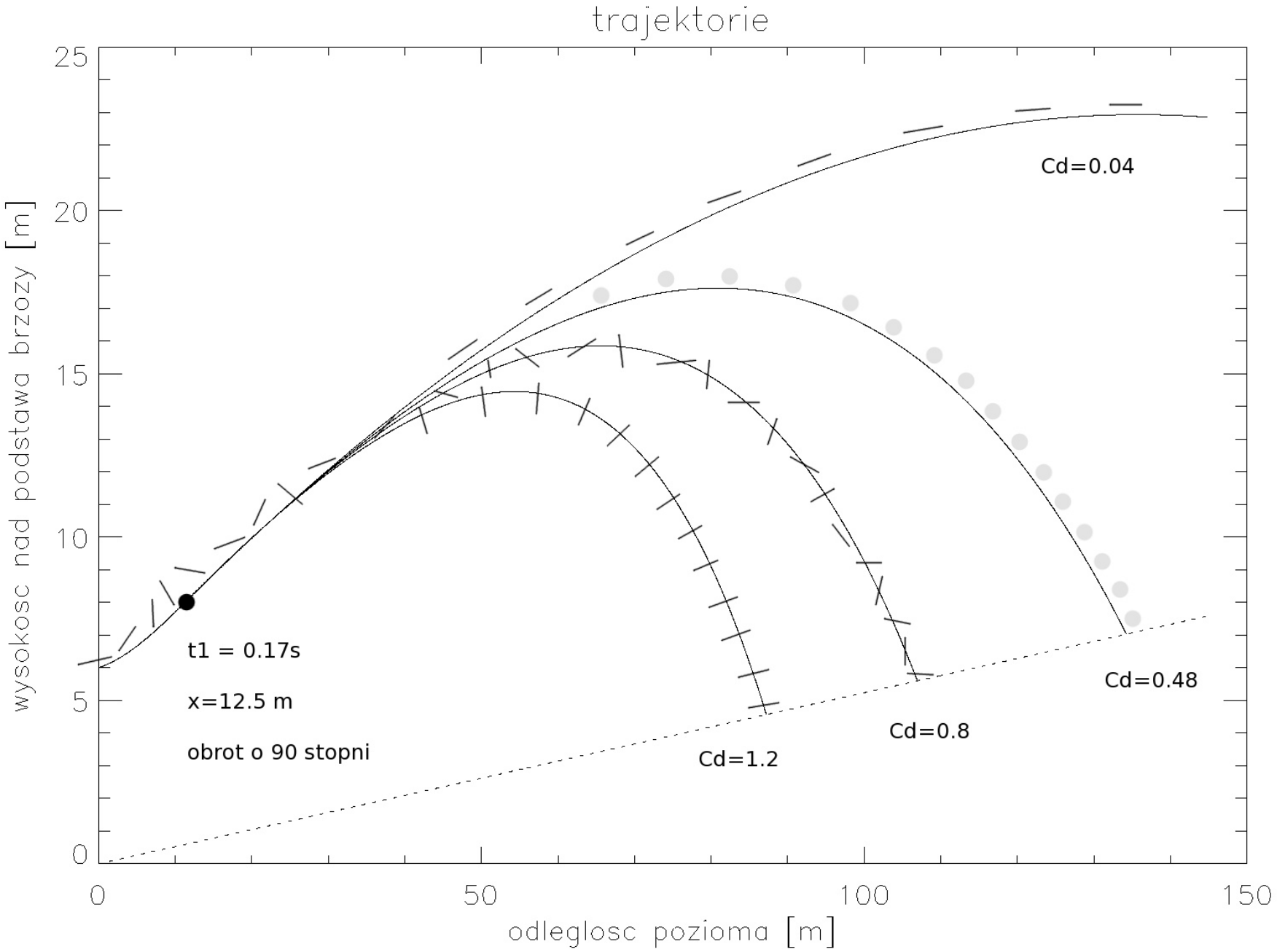

However, I recently added detailed consideration of unsteady aerodynamics, where lift and drag forces up to a few times higher than in the stabilized flow are possible.

J. Fluid Mech. (1979), *vol.* 92, *part* 2, *pp.* 327–348
Printed in Great Britain

Autorotating flat-plate wings: the effect of the moment of inertia, geometry and Reynolds number

By J. D. IVERSEN

Department of Aerospace Engineering and Engineering Research Institute,
Iowa State University, Ames

(Received 2 November 1977)

Free-flight and wind-tunnel measurements by previous investigators of the flat-plate autorotation phenomenon have been analysed. The variation of the autorotation characteristics with changes in the Reynolds number and the aspect ratio, thickness ratio and moment of inertia of the flat plate have been correlated. The interpretation of the role of the Reynolds number made in a previous investigation is shown to be incorrect. The tip-speed ratio, for the ranges of the dimensionless parameters investigated, is shown to be a function of only the plate aspect ratio, thickness ratio, and also the moment of inertia if the latter is sufficiently small. The lift and drag coefficients, and therefore the free-flight glide angle, are shown to be functions of the tip-speed ratio, the aspect ratio and the Reynolds numbers based on the chord and plate thickness.

1. The Magnus rotor: introduction

The Magnus rotor as defined here is a cylinder of arbitrary cross-section which revolves about an axis perpendicular to the cross-section and moves through air or another fluid in a direction perpendicular to this axis (or is stationed in a wind tunnel

A number of important new works have appeared recently...

J. Fluid Mech. (2013), *vol.* 733, R5, doi:10.1017/jfm.2013.444

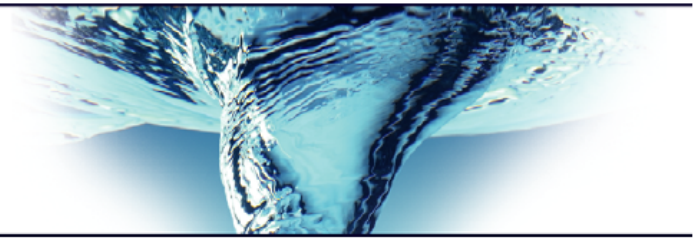

JFM RAPIDS
journals.cambridge.org/rapids

Unsteady pitching flat plates

Kenneth O. Granlund[1,†], Michael V. Ol[1] and Luis P. Bernal[2]

[1]Air Force Research Laboratory, Wright-Patterson AFB, OH 45433, USA
[2]Department of Aerospace Engineering, University of Michigan, Ann Arbor, MI 48109, USA

(Received 5 June 2013; revised 31 July 2013; accepted 19 August 2013)

Direct force measurements and qualitative flow visualization were used to compare flow field evolution versus lift and drag for a nominally two-dimensional rigid flat plate executing smoothed linear pitch ramp manoeuvres in a water tunnel. Non-dimensional pitch rate was varied from 0.01 to 0.5, incidence angle from 0 to 90°, and pitch pivot point from the leading to the trailing edge. For low pitch rates, the main unsteady effect is delay of stall beyond the steady incidence angle. Shifting the time base to account for different pivot points leads to collapse of both lift/drag history and flow field history. For higher rates, a leading edge vortex forms; its history also depends on pitch pivot point, but linear shift in time base is not successful in collapsing lift/drag history. Instead, a phenomenological algebraic relation, valid at the higher pitch rates, accounts for lift and drag for different rates and pivot points, through at least 45° incidence angle.

The Fifth International Symposium on Computational Wind Engineering (CWE2010)
Chapel Hill, North Carolina, USA May 23-27, 2010

Aerodynamic Characterisation of Static and Auto-rotating plates using coupled CFD-RBD simulations

Bruce Kakimpa [a], David M. Hargreaves [b], John S. Owen [c]

[a] *Postgraduate Research Student, Department of Civil Engineering, University of Nottingham, UK, evxbk1@nottingham.ac.uk*
[b] *Lecturer, Department of Civil Engineering, University of Nottingham, UK, david.hargreaves@nottingham.ac.uk*
[c] *Associate Professor, Department of Civil Engineering, University of Nottingham, UK, john.owen@nottingham.ac.uk*

ABSTRACT: The phenomenon of plate autorotation is one that has application in a number of practical problems. Previous experimental investigations of autorotation have however been focused on single degree of freedom autorotation about a fixed axis due to the practical difficulties involved with implementing full 3D autorotation. Numerical studies of the problem have also focused mainly on 2D and low Reynolds number problems with one rotational degree of freedom. However in many practical situations, autorotation is three-dimensional in nature, exhibiting non-linear three degree of rotational freedom autorotation about an arbitrary axis. A more complete numerical treatment of autorotation is therefore necessary. This paper presents a three-degree of freedom simulation of the autorotation of a 3D low aspect ratio plate about its centre of mass in a high Reynolds number flow using a coupled CFD-RBD approach. The effects of vortex shedding on plate motion are found to be negligible and the autorotation phenomenon is found to be strongly dependent on the initial orientation of the plate. Predicted autorotational velocities are found to agree with experimentally derived correlation expressions.

The autorotation occurs at AR (elongation factors) in a wide range, for instance in case of flat square pieces. The phenomenon is insensitive to Reynolds number Re.

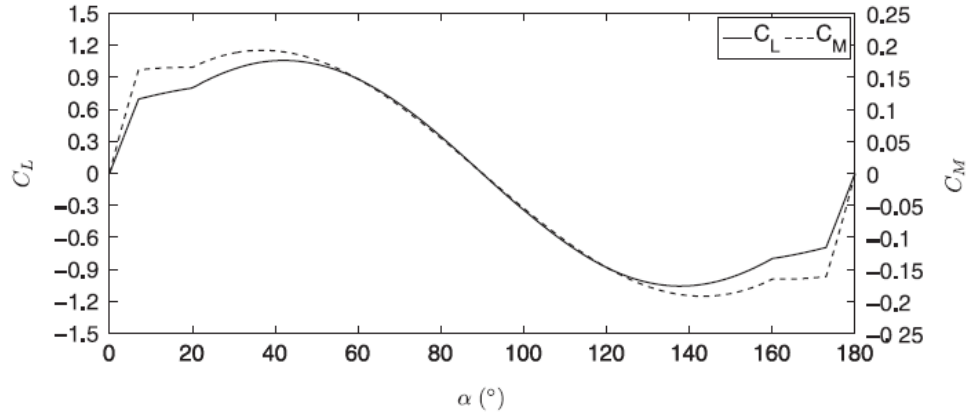

Fig. 1. Steady-state curves showing the variation of lift, C_L, and moment, C_M, coefficients with angle of attack, α for static square flat plates held in a steady flow (ESDU, 1970).

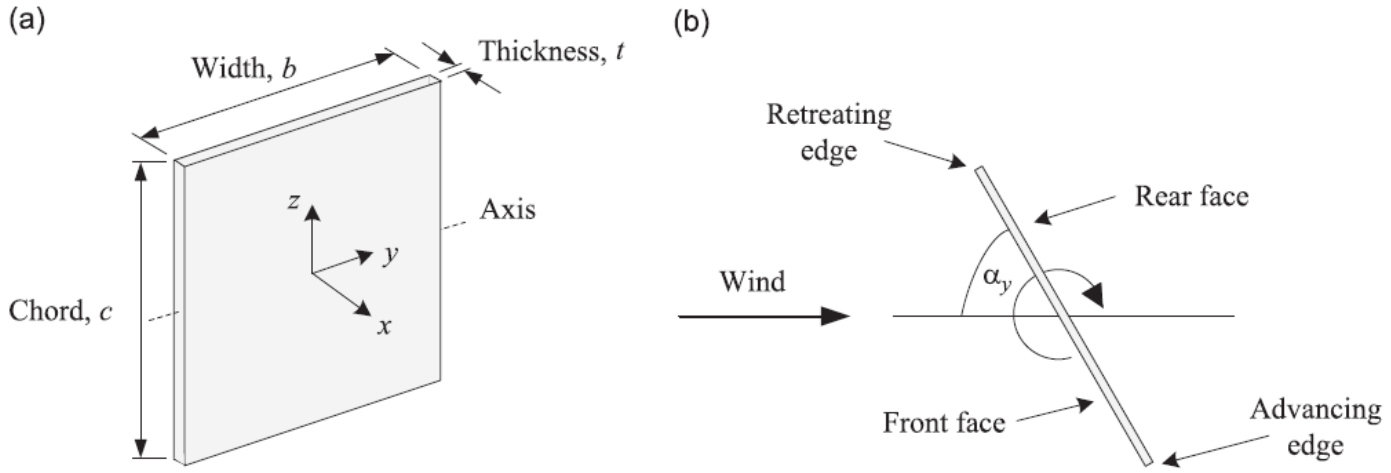

Fig. 2. (a) Dimensions and orientation of the plate and (b) the nomenclature associated with an autorotating plate.

Non-stationary airfoil aerodynamics;
Autorotation is caused by a lowered pressure of the vortex behind the leading edge. Autorotation prefers a speed of rotation such that the linear rotation speed of the edge equals 0.35-0.5 of the speed of the undisturbed, incoming airflow

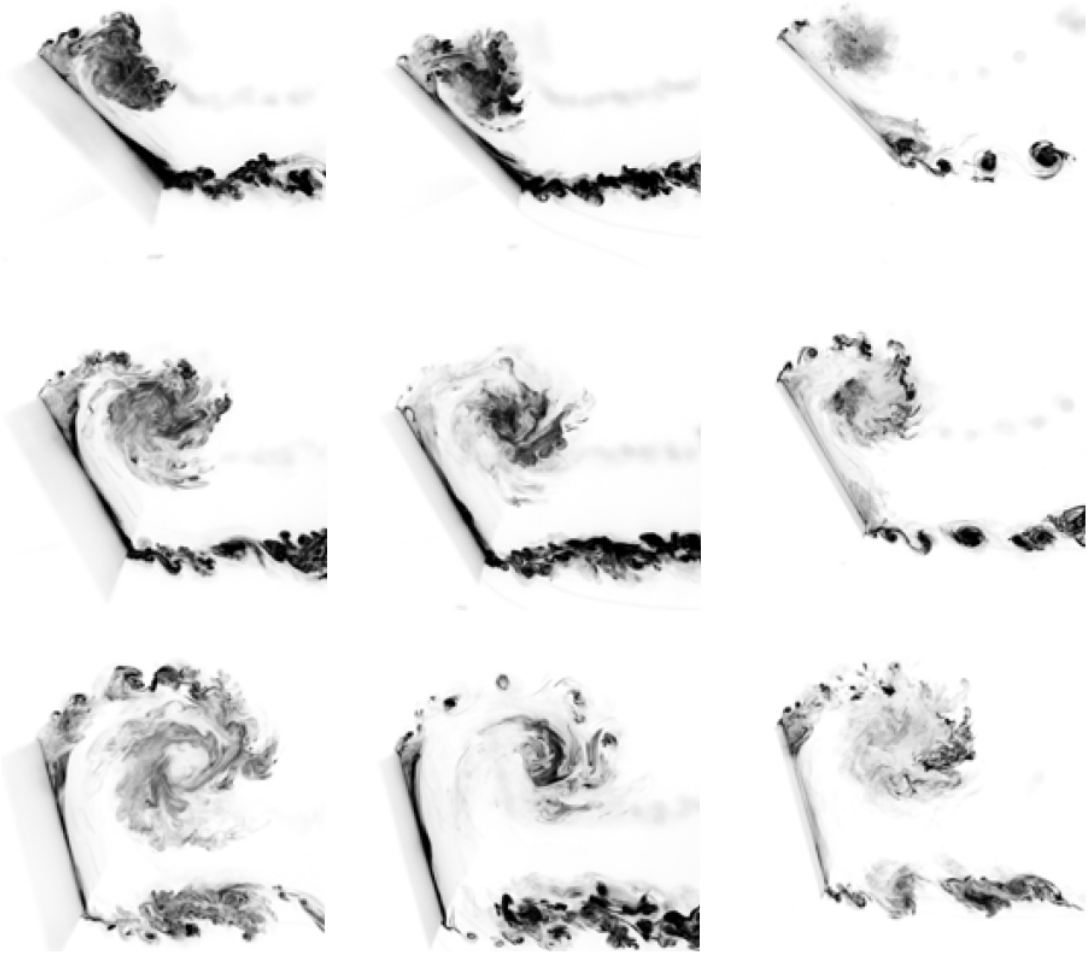

xample of detailed calculation

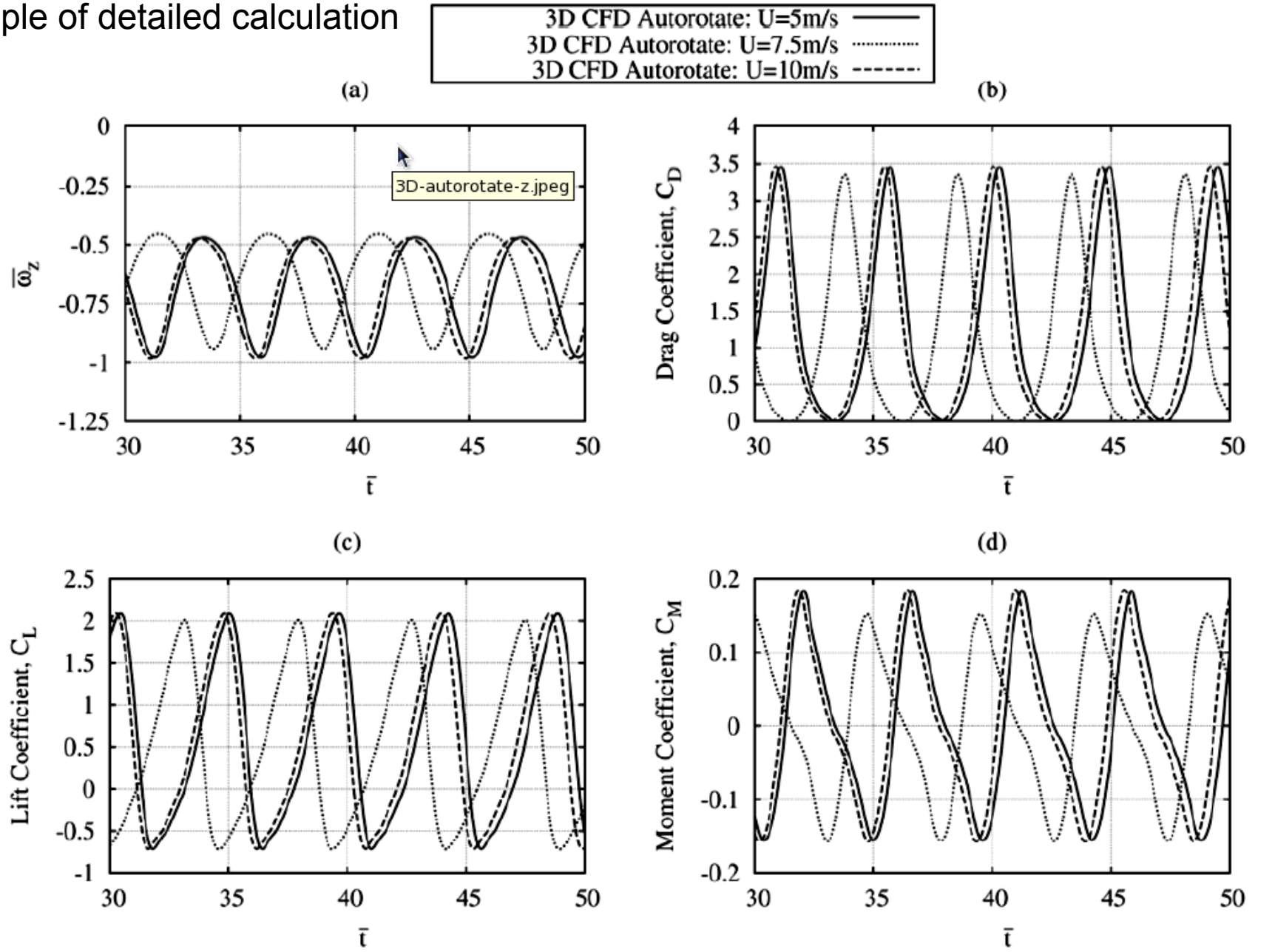

Figure 5: Time series plots for autorotational speed (a), drag coefficients (b), lift coefficients (c) and moment coefficients (d), obtained from 3D CFD-RBD simulations performed at various wind speeds

Free flight of the plate: rotation around the long axis with nutation

4.3 *Free-Axis Autorotation*

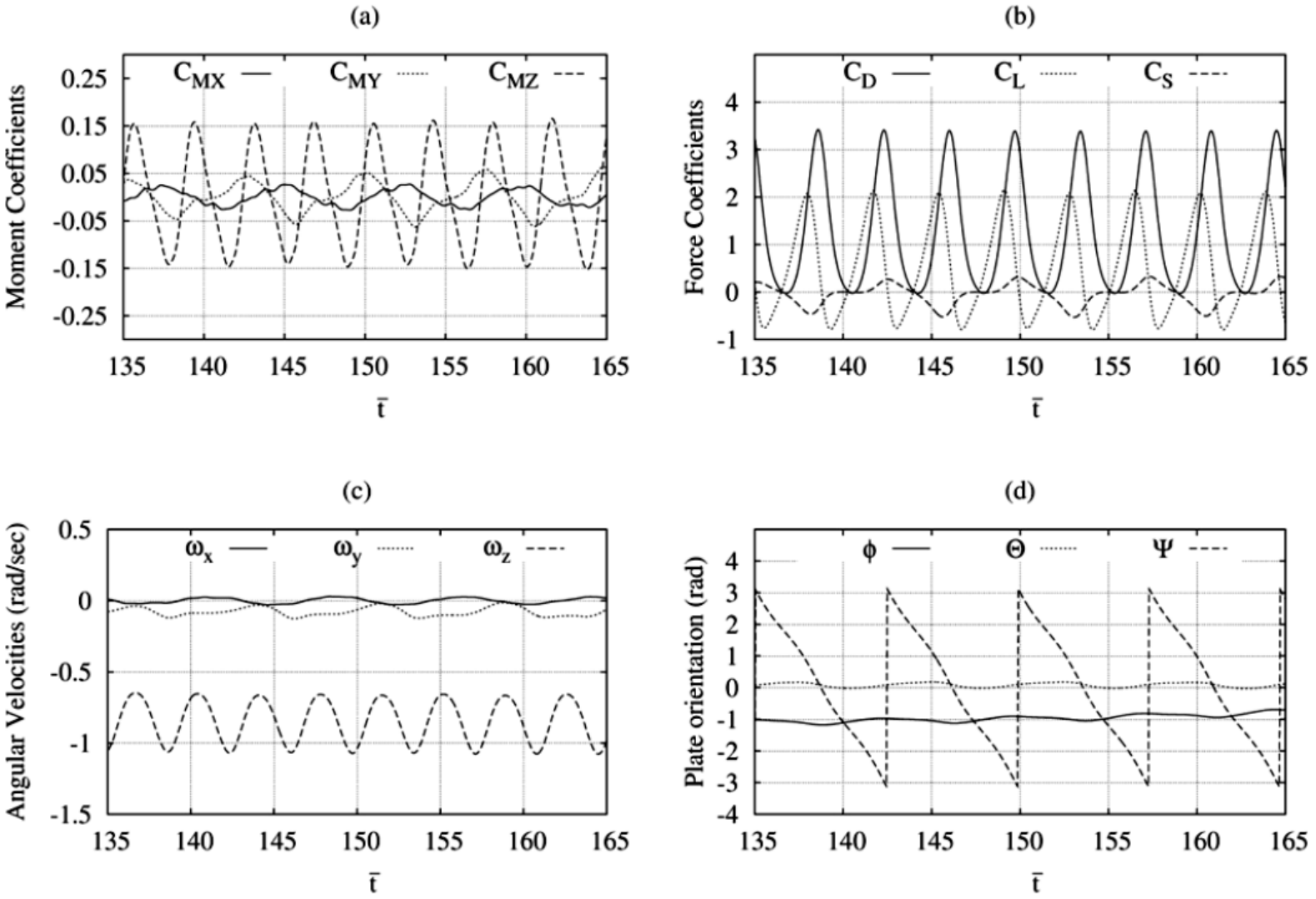

Figure 7: Moments (a), Forces (b), Angular velocities (c) and Orientation (d) from CFD-RBD simulations of a plate autorotating freely about an arbitrary axis through its centre of mass.

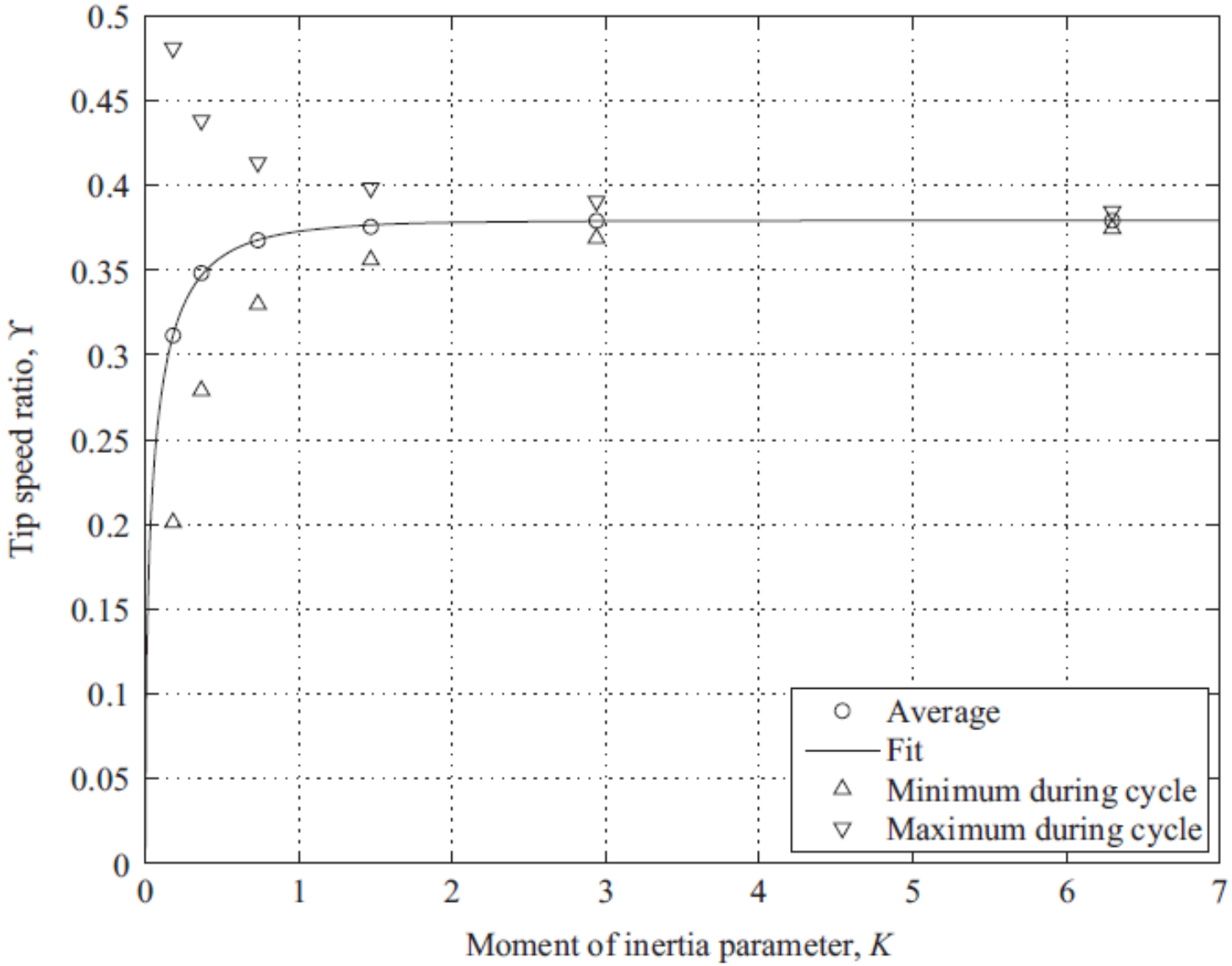
Tip speed ratio, Υ
Moment of inertia parameter, K
0
0.05
0.1
0.15
0.2
0.25
0.3
0.35
0.4
0.45
0.5
0
1
2
3
4
5
6
7
Average
Fit
Minimum during cycle
Maximum during cycle

unsteady flow results in lift force insensitive to viscosity (Re number)

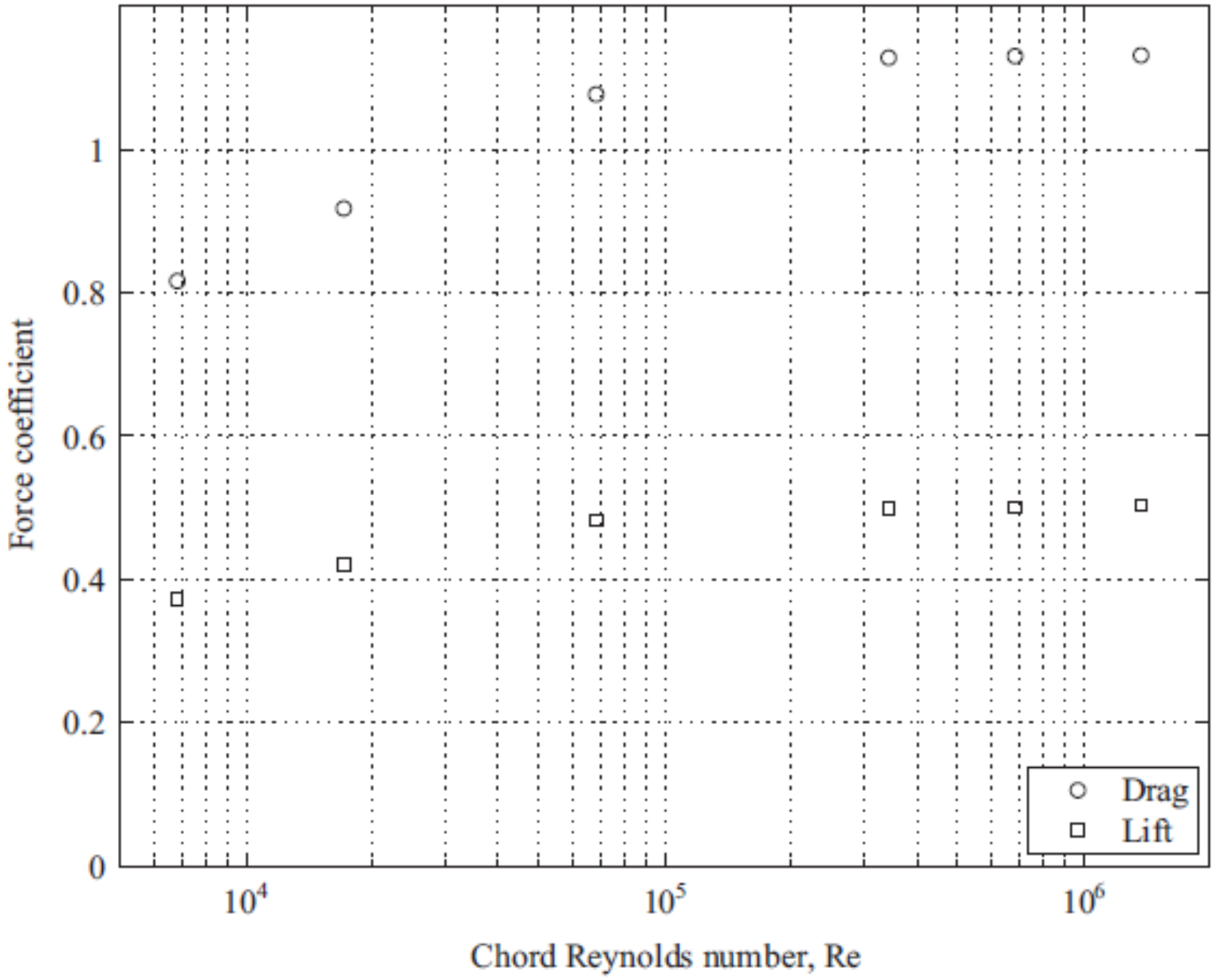

Journal of Fluids and Structures 46 (2014) 111–133

Contents lists available at ScienceDirect

Journal of Fluids and Structures

journal homepage: www.elsevier.com/locate/jfs

The computational fluid dynamics modelling of the autorotation of square, flat plates

D.M. Hargreaves*, B. Kakimpa, J.S. Owen

Faculty of Engineering, University of Nottingham, Nottingham NG7 2RD, UK

ARTICLE INFO

Article history:
Received 9 August 2012
Accepted 1 December 2013
Available online 14 February 2014

Keywords:
CFD
Autorotation
Fluid–structure interaction

ABSTRACT

This paper examines the use of a coupled Computational Fluid Dynamics (CFD) – Rigid Body Dynamics (RBD) model to study the fixed-axis autorotation of a square flat plate. The calibration of the model against existing wind tunnel data is described. During the calibration, the CFD models were able to identify complex period autoration rates, which were attributable to a mass eccentricity in the experimental plate. The predicted flow fields around the autorotating plates are found to be consistent with existing observations. In addition, the pressure coefficients from the wind tunnel and computational work were found to be in good agreement. By comparing these pressure distributions and the vortex shedding patterns at various stages through an autorotation cycle, it was possible to gain important insights into the flow structures that evolve around the plate. The CFD model is also compared against existing correlation functions that relate the mean tip speed ratio of the plate to the aspect ratio, thickness ratio and mass moment of inertia of the plate. Agreement is found to be good for aspect ratios of 1, but poor away from this value. However, other aspects of the numerical modelling are consistent with the correlations.

The dashed line shows a slow stabilization of rotation rate after many full turns for a dimensionless coefficient of the moment of inertia appropriate for the detached wingtip of PLF 101 (timescale, however, relates to a different, published model)

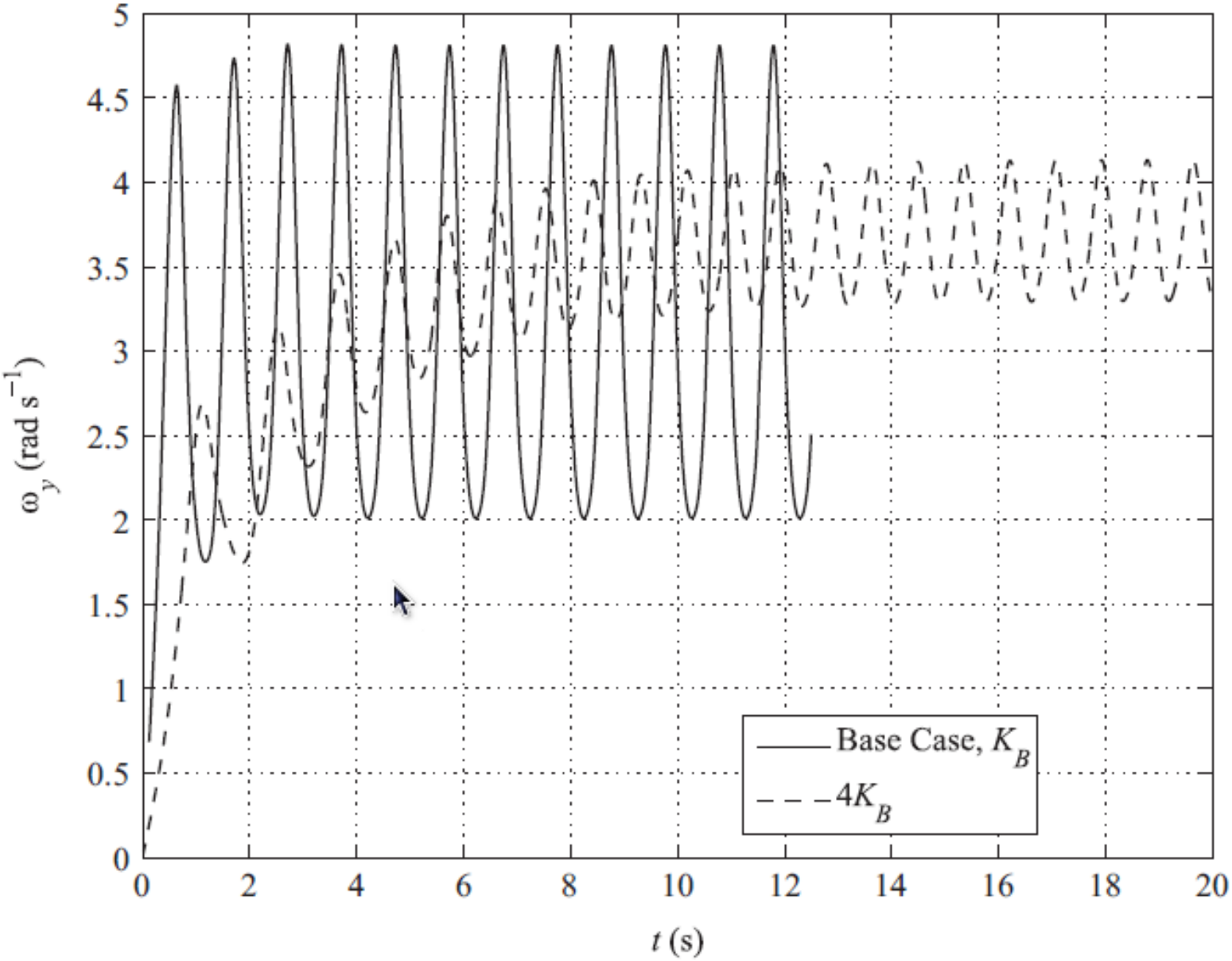

Cd, CL and Cm as a function of the angle of attack of autorotating airfoil

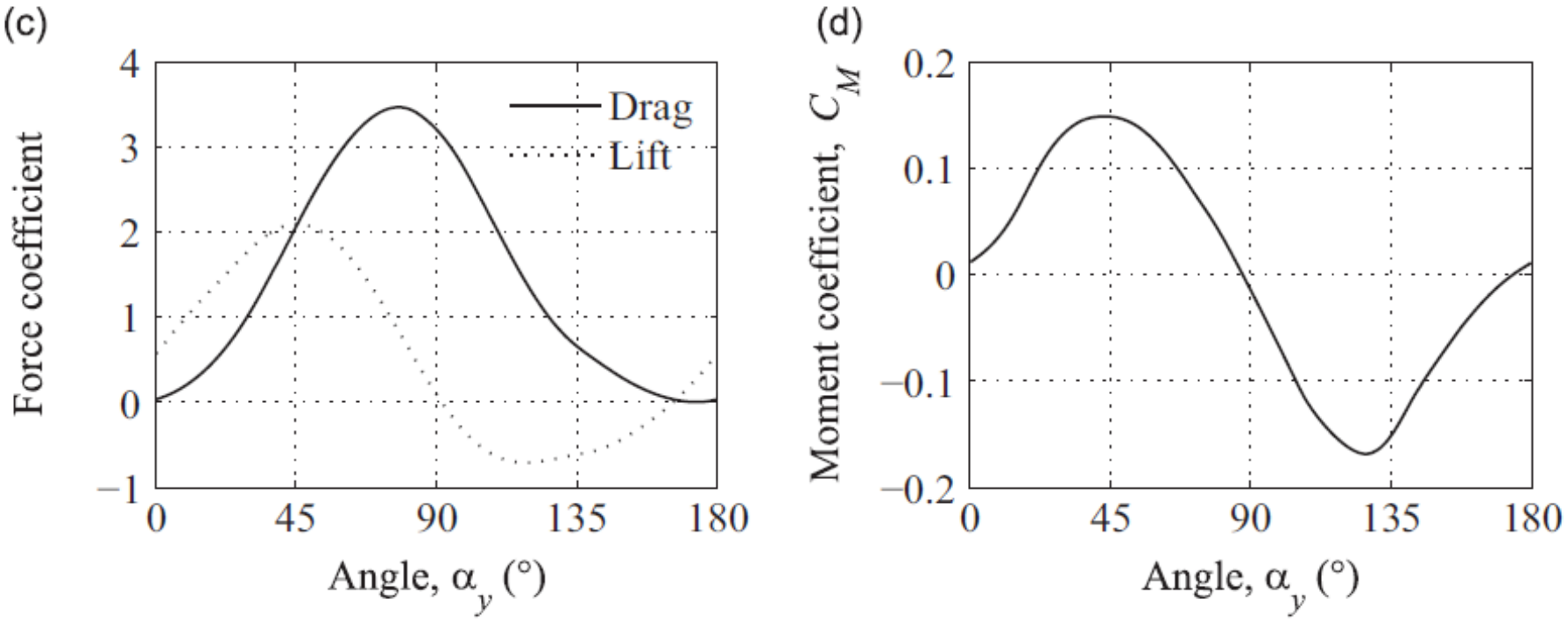

CL and Cd coefficients (as a function of the angle of attack) during autorotation of the wingtip of Tupolev PLF 101

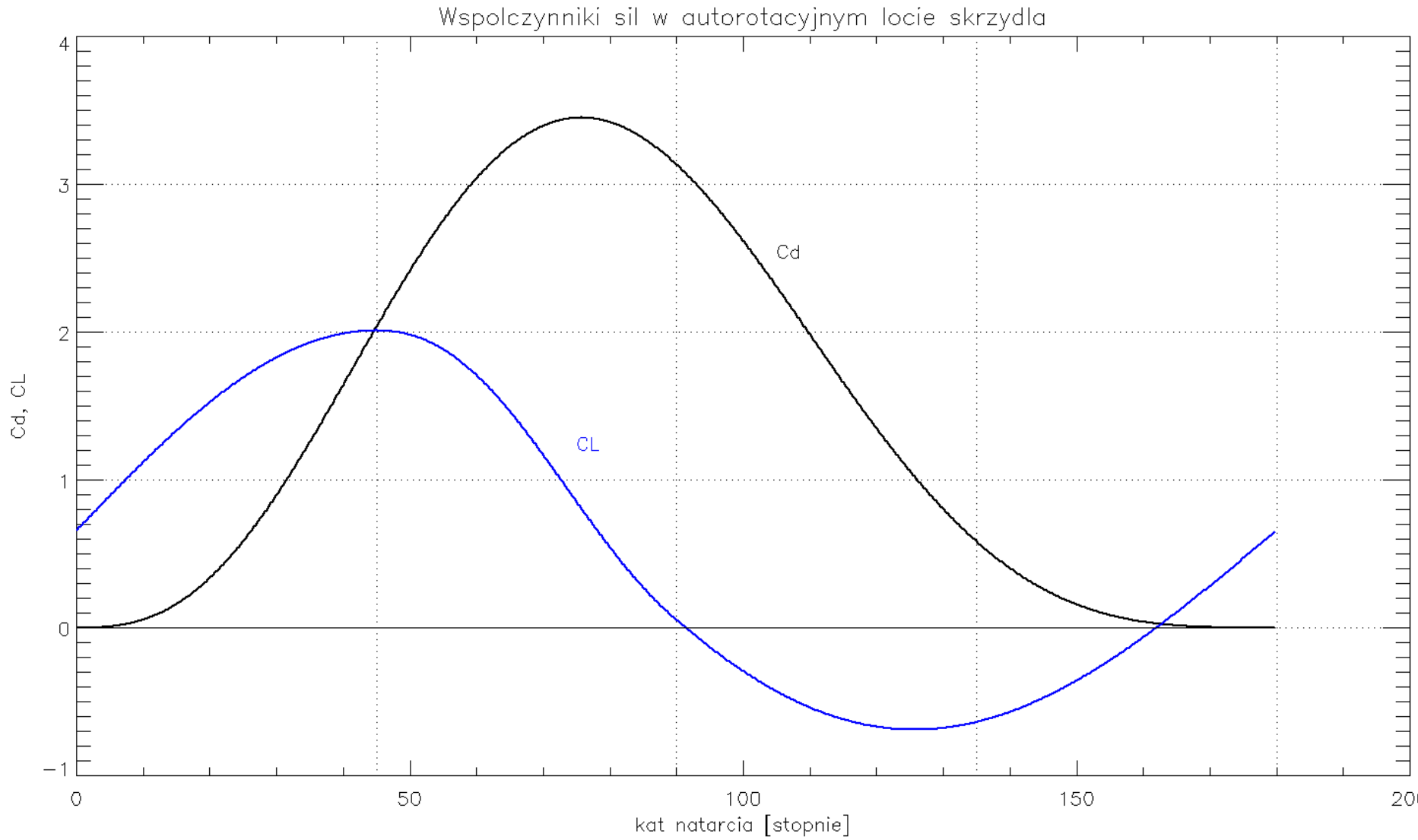

Numerical trajectory and the rotation of the wingtip, taking into account autorotation, drag force and the Magnus (lift) force

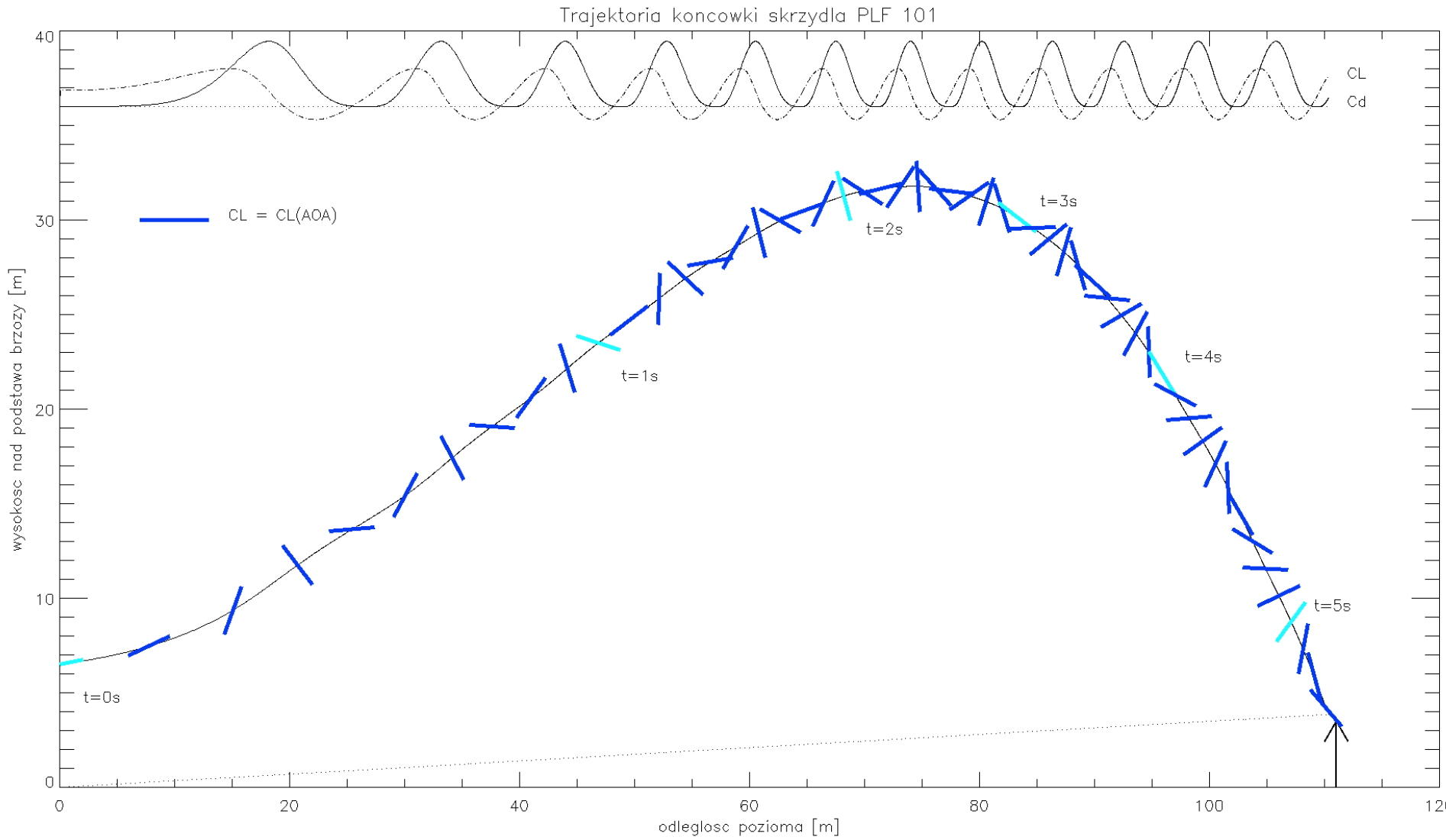

Comparison of flight with and without Magnus' effect

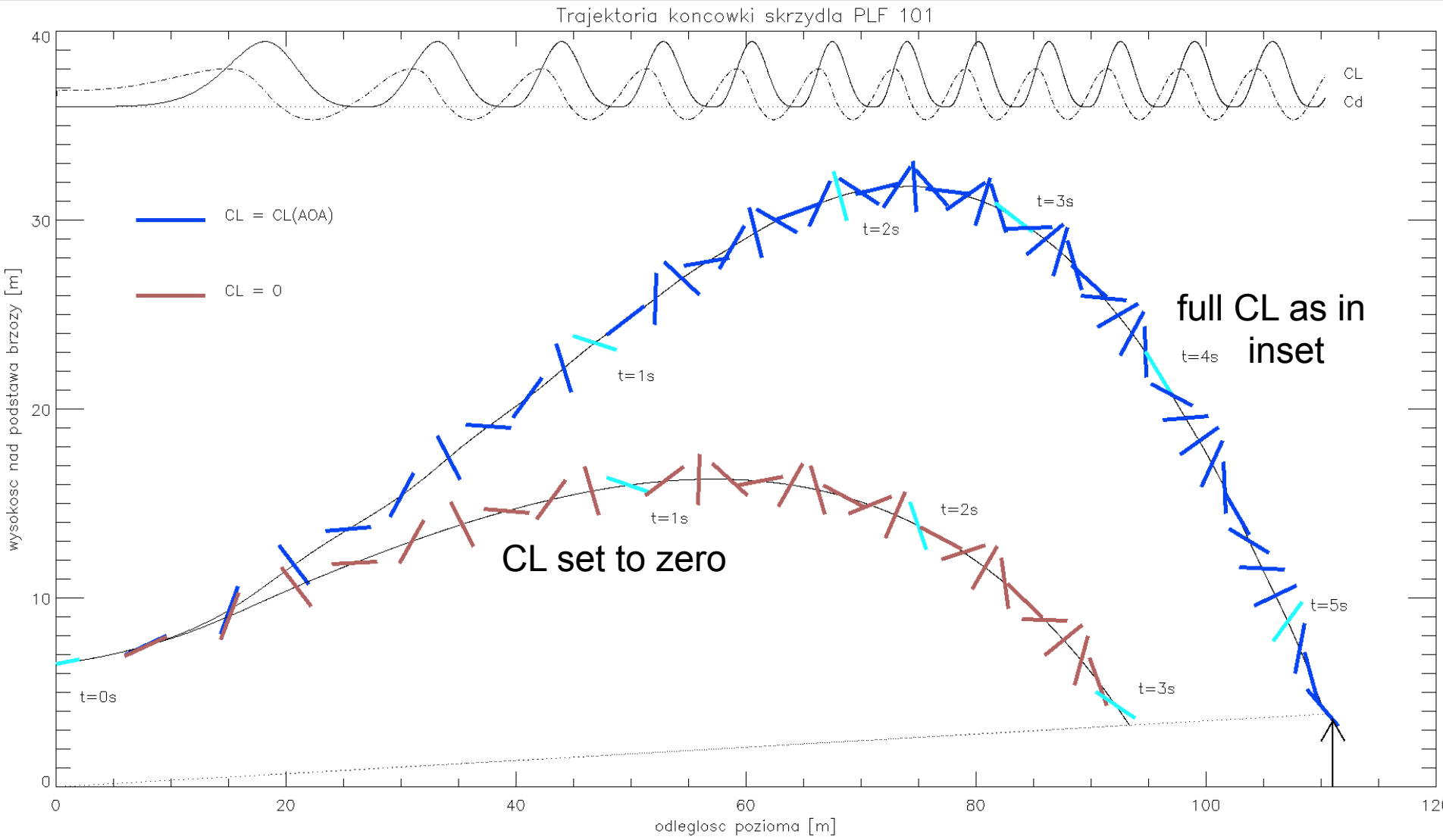

Conclusions about the wingtip trajectory: the wingtip:

- rapidly accelerated up and began autorotating
- It flew for about 5 seconds, rotating along its long axis with some nutation
- It fell after covering about 110 m distance with velocity not larger than ~70 km/h, at a ~50 degrees angle to the horizon

- Agreement with the reality as found by post-accident investigations is very good.

Part II of the presentation:

How was the outer part of the wing detached?

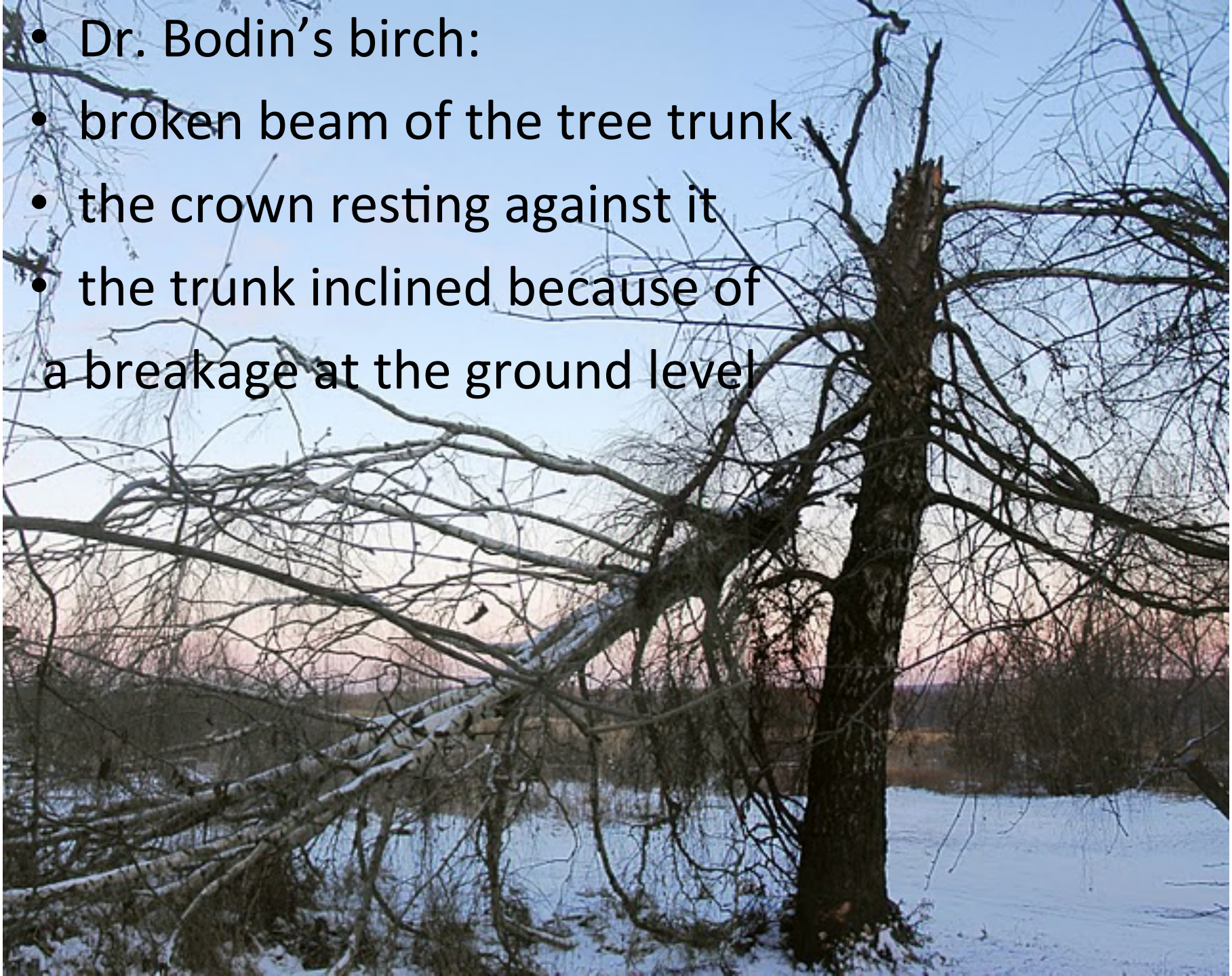

- Dr. Bodin's birch:
- broken beam of the tree trunk
- the crown resting against it
- the trunk inclined because of a breakage at the ground level

Facts about Bodin's birch:

no missing sector of a trunk, potentially crushed by a wing.

In 2012 the military prosecutor's office physically reconstructed most of the beam of the birch from the broken parts, which fit together without much timber loss.

Tree trunk after collision has up to 1 m-long splinters. It was not cut or crushed sector-wise, but broken at moderate speed. The position of the tree top shows the direction of collision that has bent the birch beyond the modulus of rupture (MOR) of fibers.
The tree was dynamically hit in by a slanted wing of west-moving aircraft.

Trunk's inclination

.is due to a split (breakage)
at its bottom, on the side from which the tree was hit.

.

The double breakage on opposite sides of the trunk are a sure sign of a dynamic bending

Typical data about the wood

Pergamon

Int. J. Impact Engng, Vol. 19, Nos. 5–6, pp. 531–570, 1997

0734-743X/97 $17.00+0.00

PII:S0734-743X(97)00016-X

DYNAMIC UNIAXIAL CRUSHING OF WOOD

S.R. REID* and C. PENG

Department of Mechanical Engineering, UMIST, PO Box 88, Sackville Street, Manchester, M60 1QD, U.K.

(*Received* 30 *October* 1996; *in revised form* 30 *January* 1997)

EXPERIMENTAL RESULTS

Mechanical properties at the static loading.

The testing of wood under static loading in tension, pressure and in bending represents a standard procedure. Owing to this fact, no description of these experiments is presented. The results of this testing are given in Table 1.

Table 1. Strengths of the tested woods. (ME – modulus of elasticity in MPa, MR – modulus of rupture in MPa)

WOOD	Density (kg/m^3)	Strength in tension ∥ (MPa)	Strength in tension ⊥ (MPa)	Strength in pressure ∥ (MPa)	Strength in pressure ⊥ (MPa)	MR	ME	Toughness J/cm^2
Spruce	440	84	1.5	30	4.1	60	9 100	4.9
Pine	530	102	2.9	54	7.5	98	11 750	6.9
Oak	700	108	3.3	42	11.5	116	11 600	7.4
Beech	720	130	3.5	46	[illegible]	[illegible]	[illegible]3 100	7.8
Birch	730	134	6.9	50	10.8	134	[illegible]6 100	6.6

Table 1. Numbers of specimens measured (N), means, standard deviations and the outermost values for the specific gravity (ρ_{12}), MOE and MOR for *Betula pendula* and *B. pubescens*. Below the Pearson correlations between the study variables by species

Species (N)	*B. pendula* (249)			*B. pubescens* (361)		
	ρ_{12}	MOE, GPa	MOR, MPa	ρ_{12}	MOE, GPa	MOR, MPa
Mean	565.9	14.5	113.9	538.1	13.2	104.1
Std. deviation	38.7	2.1	14.8	35.7	1.9	14.1
Min	440.1	7.8	69.8	456.9	8.2	61.3
Max	687.3	19.9	156.6	640.8	20.0	141.4
Pearson correlations						
ρ_{12}	1.000			1.000		
MOE, GPa	0.694	1.000		0.663	1.000	
MOR, MPa	0.827	0.877	1.000	0.792	0.860	1.000

Table 2. Bending properties of birch wood, species combined. A comparison of the means of the current study with those presented in the literature

Characteristics	Current study	Jalava (1945)	Wagenführ (1996)	Dunham et al. (1999)	
	Small clears	Small clears	Small clears	Small clears	Sawn wood
MOE, GPa	13.7	14.1–15.4	14.5–16.5	8.5–14.0	8.2–13.3
MOR, MPa	108.1	98.6–110.9	76–155	93.1–132.3	46.6–64.3

Behavior of wood under tension (modulus of rupture MOR) vs. compression

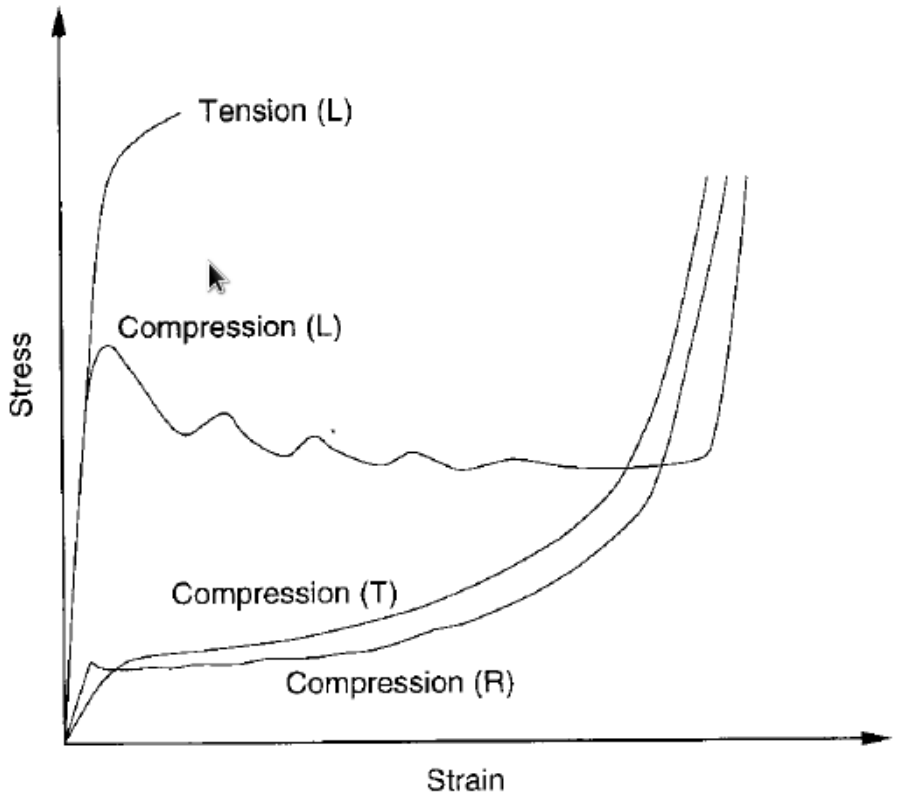

Fig. 9. Typical stress–strain curves for wood loaded in compression in the longitudinal, radial and tangential directions and for tension in the longitudinal direction.

Wood cells were being crushed following the first contact with the wing. About 15 percent of the trunk sector was crushed by the wing. Afterwards, the contact area grew and the stress values dropped below the timber crushing limit. The tree meanwhile started being deflected as a whole and the wing started fragmenting after buckling and exceeding locally the metal yield stress.

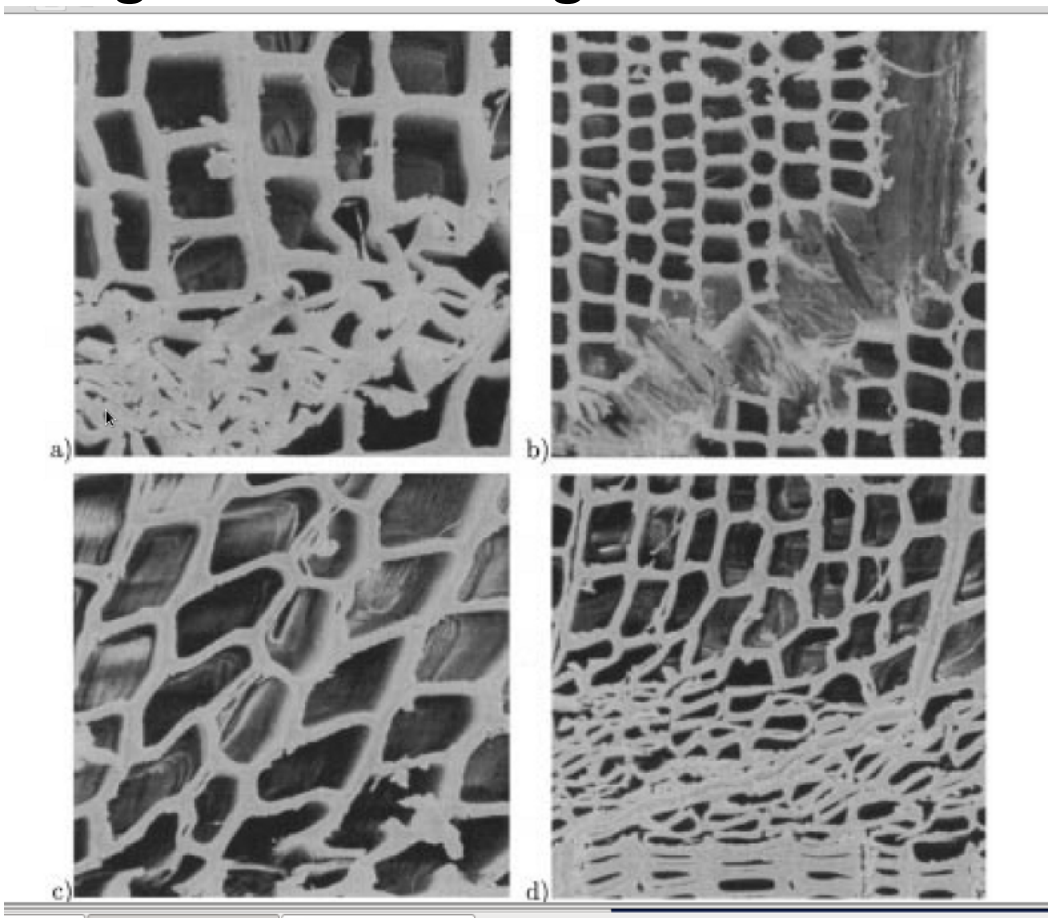

Estimates of birch wood and oak strengths

Table 1. Uniaxial quasi-static parameters for wood specimens tested under laterally constrained conditions (uniaxial compression); 75 mm diameter × 75 mm high

Wood and grain orientation	Initial density, ρ_0 (kg m^{-3})	Initial crush stress, σ_{cr} (N mm^{-2})	Theoretical crush stress, Eqns (1) or (2) (N mm^{-2})	Locking strain, ε_l	Specific locking energy (kJ kg^{-1})
Balsa 0°	277	27.0	27.7	0.68	63.4
Balsa 90°	264	1.6	2.2	0.65	10
Y. Pine 0°	383	43.3	38.3	0.64	62.2
Y. Pine 90°	396	5.1	4.9	0.60	15.2
Redwood 0°	367	43.0	36.7	0.65	59.0
Redwood 90°	409	10.5	5.2	0.58	16.3
A. Oak 0°	725	75.0	72.5	0.33	30.4
A. Oak 90°	695	12.3	15.0	0.37	16.0
Ekki 90°*	1051	24	34.4	—	—
Ekki 90°	1183	18.2	43.5	0.13	3.7

MPa

* Free specimen.

Zgniatanie powolne

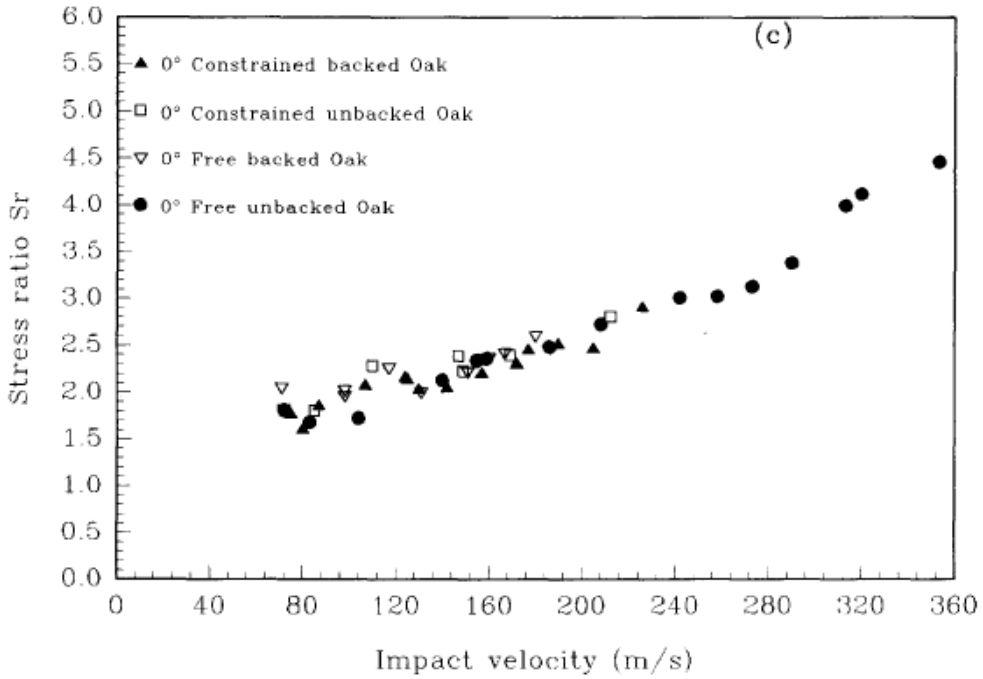

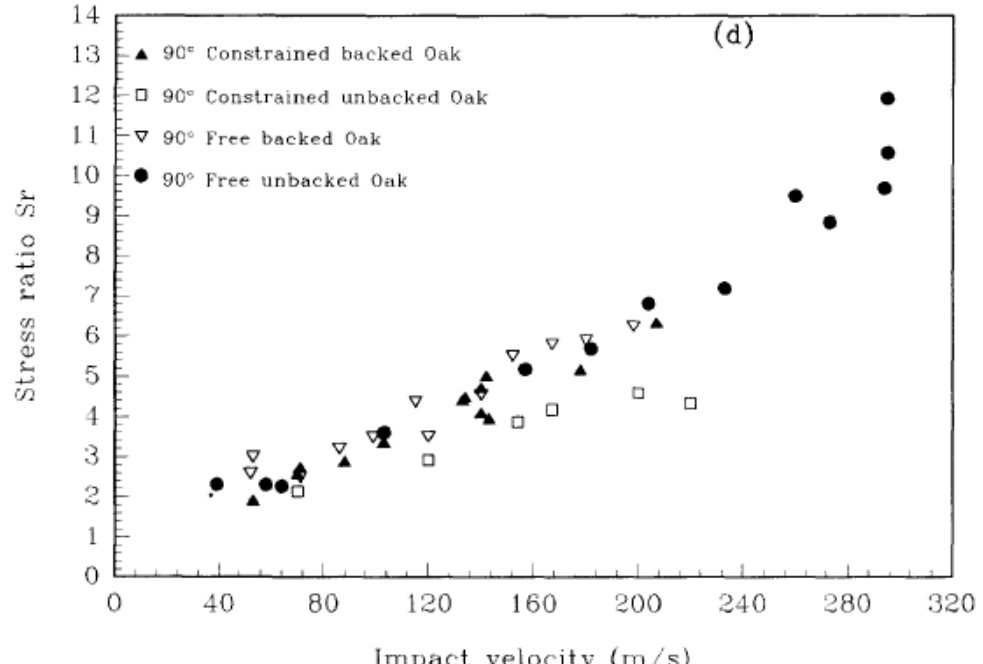

Rapidly crushed wood is much (~2 x) tougher than a slowly deformed wood.

Modeling with LS-Dyna requires the knowledge of these typical issues with an FEM method

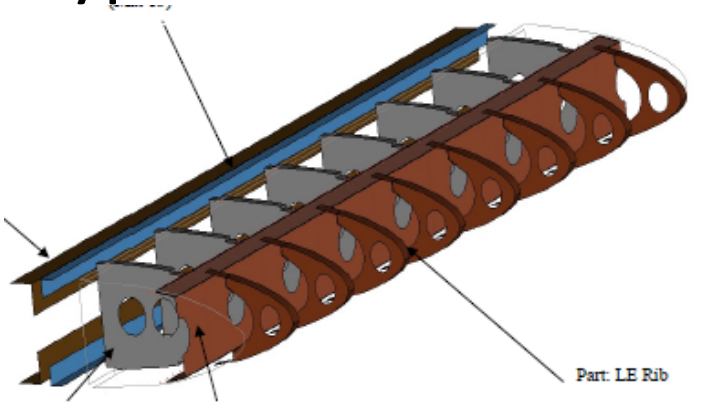

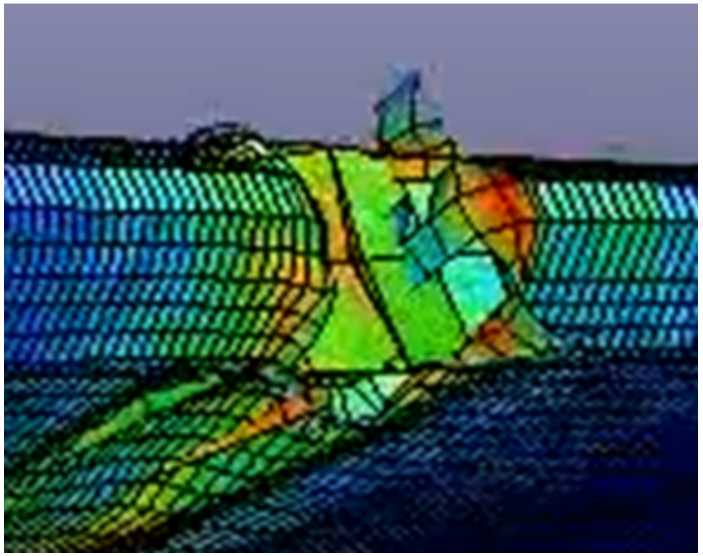

One of Binienda's models compared with a more realistic internal structure of the wing)

1. High resolution is a must
2. Beware of numerical erosion of FEM elements in dynamical situations. Conservation laws are violated if timber disappears, wing is not even challenged, tree inertia disappears
3. When time-step inexplicably drops to a rock-bottom value 1 ns in a low-res LS-Dyna sim (to cross 1 FEM tree cell the wing takes ~10000000 time-steps!), the calculation is NOT accurate. It no longer makes sense. This could be due to excessive mesh distortion or hourglassing or something else.
4. Never overestimate the D16 alloy's thickness, especially by a factor of 3-4

Available online at www.sciencedirect.com
SCIENCE DIRECT®
ELSEVIER
International Journal of Impact Engineering 32 (2005) 188–209
INTERNATIONAL JOURNAL OF IMPACT ENGINEERING
www.elsevier.com/locate/ijimpeng

there is one more thing – standard material models do not take this into account:

Review on critical impact velocities in tension and shear

J.R. Klepaczko

Metz University, Laboratory of Physics and Mechanics of Materials, UMR-CNRS 7554, Ile du Saulcy, F-57045 Metz, Cedex 01, France

Received 22 September 2004; received in revised form 23 August 2005; accepted 24 August 2005
Available online 24 October 2005

(they lower the toughness of aluminum alloys, and have been exceeded in Smolensk)

Abstract

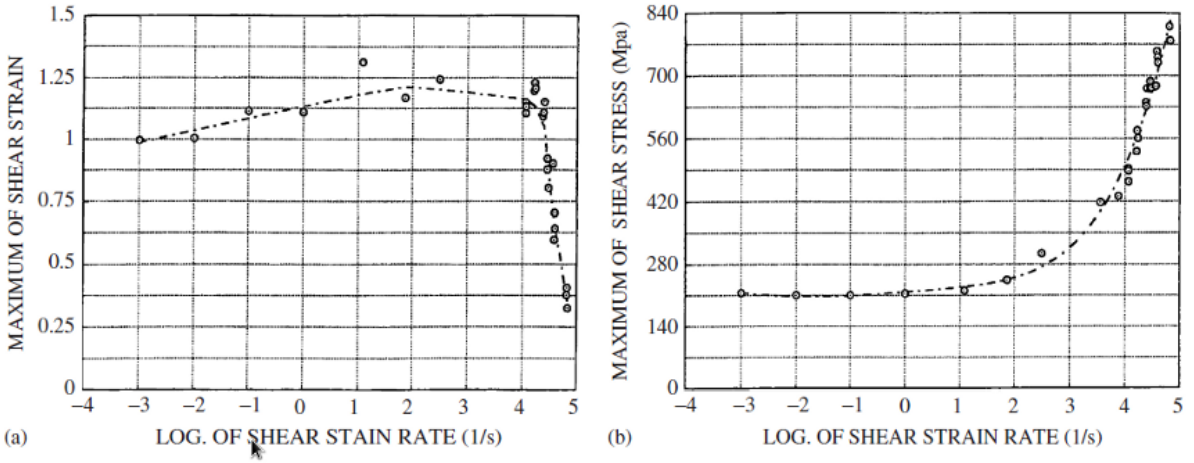

Fig. 15. Experimental results of slow and fast shearing for a hot rolled armor steel by the MDS technique: a—maximum shear strain at failure versus nominal strain rate; b—maximum shear stress versus nominal strain rate [10].

measured by the non-contact optical transducer 8 and by the black and white target 6. In addition, since the front of the striker is black the displacement of the contact striker-specimen can be also measured. The theory

Calculations of Binienda et al. (2012) – fully plastic tree (GHARD=0 !), totally unrealistic trunk bending

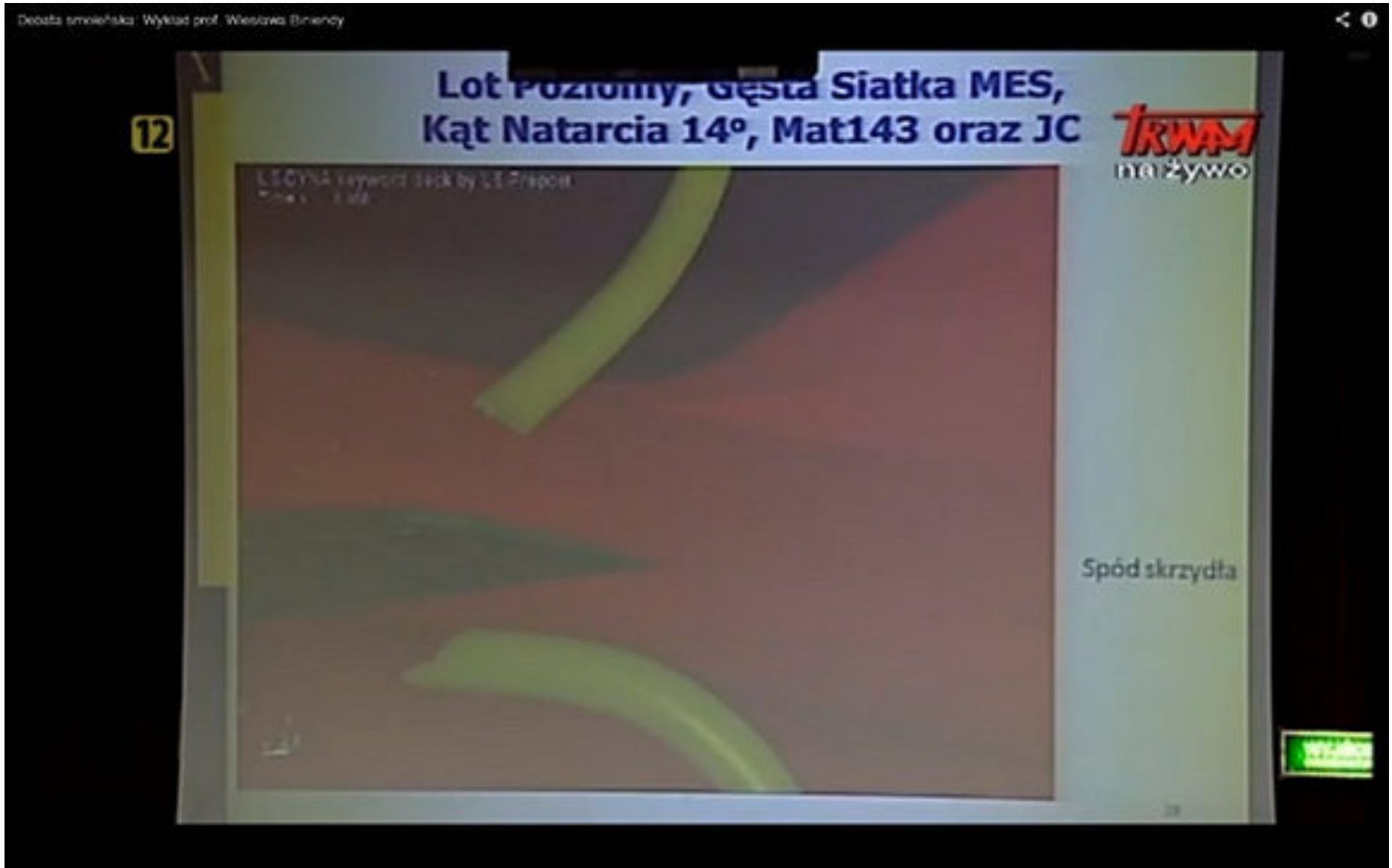

Example of correct usage of LS-Dyna: A. Morka et al (2013)

drewna brzozy i stopu aluminium, odnalezienie danych nie było możliwe. Dlatego też zadano różne współczynniki tarcia (μ=0,1 oraz μ=0,5). W wariantach H1 oraz H2 przyjęto otwory w użebrowaniu, grubość ścianki 2mm oraz EPS=0,1. Wykresy na Rys. 13 dają zbliżone wyniki. Oznacza to, że w procesie niszczenia tarcie pełni rolę drugoplanową.

Pomimo obecności perforacji w żebrach, na których rozpięto poszycie skrzydła, z dokumentacji trudno określić ich faktyczne gabaryty. Ponieważ do określenia wymiarów otworów użyto jedynie prostej proporcji, model poddano badaniu pod kątem zależności siły w miejscu kontaktu od ich średnicy. Zastosowano dwa zupełnie skrajne przypadki, pierwszy, w którym otwory są obecne oraz drugi, w którym nie występują. Wykres na Rys. 14. wykazuje pewne różnice w wielkości siły, jednak nie są one znaczące. Ponieważ wątpliwa jest jedynie kwestia wielkości i usytuowania perforacji żeber, a nie ich obecność można wnioskować, że model nie jest wrażliwy na te uproszczenia.

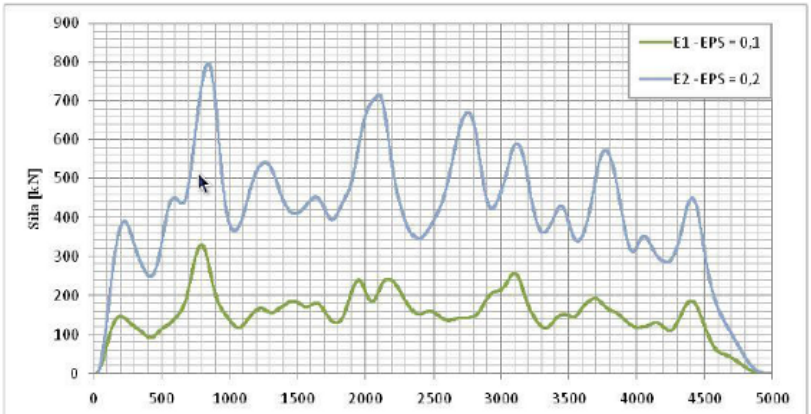

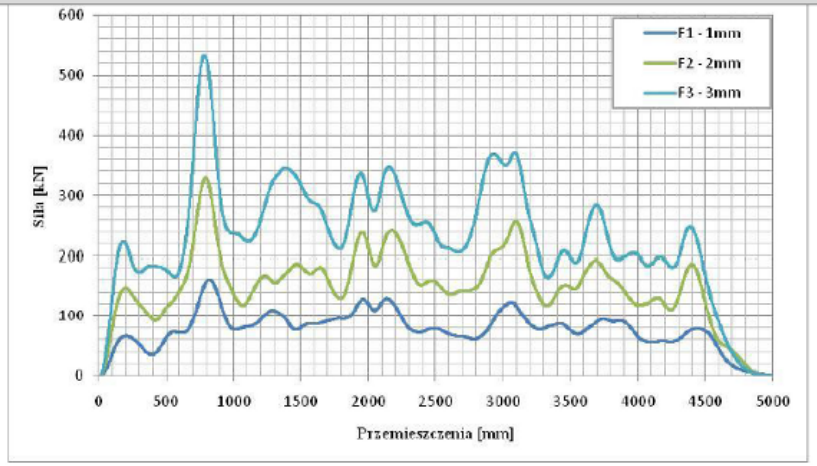

Rys. 11. **Zależność siły oddziaływania skrzydła na belkę penetrującą w funkcji jej przemieszczenia dla trzech grubości** struktury

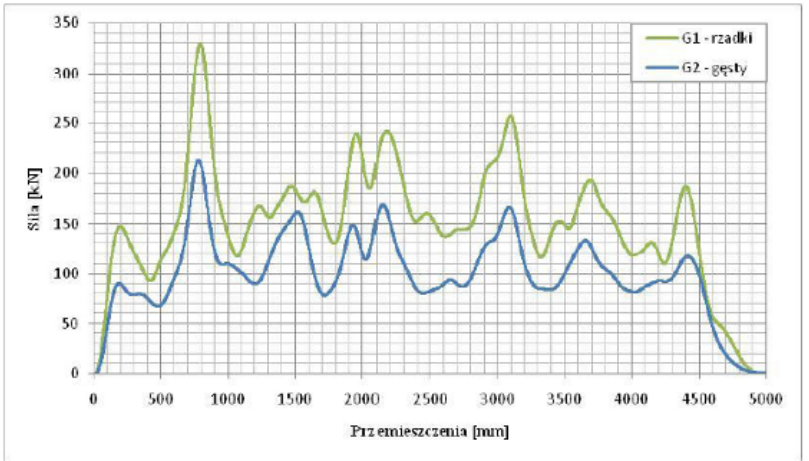

Morka et al (2012) = correct geometry of the wing

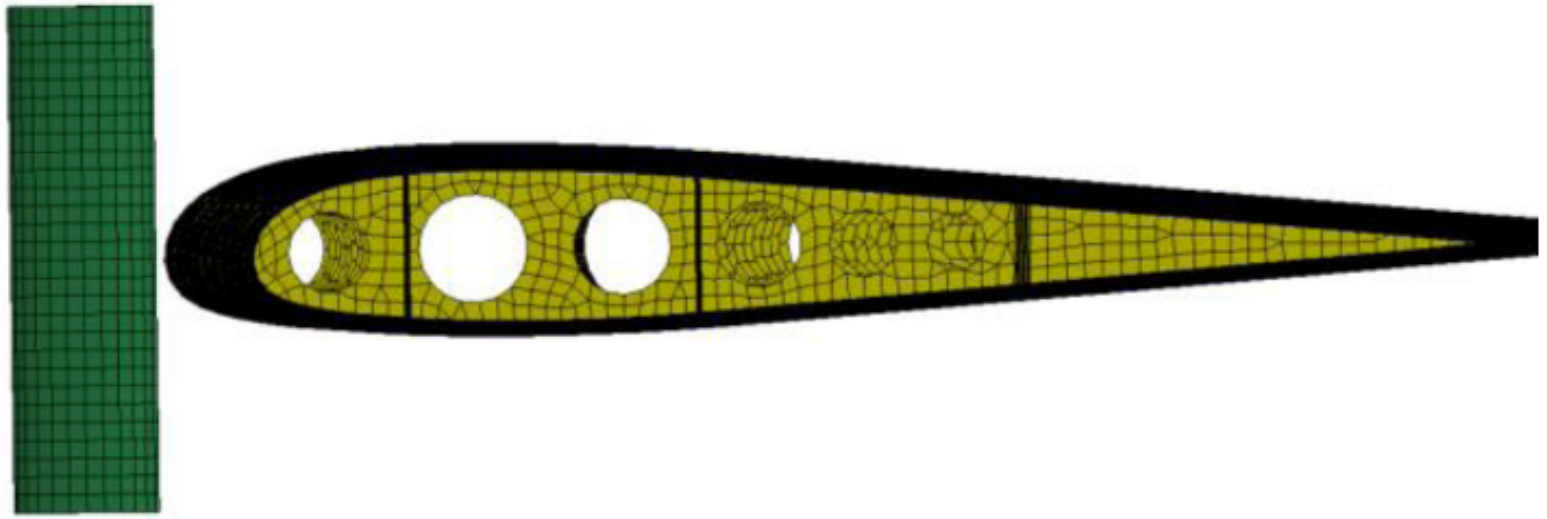

Rys. 8. **Model skrzydła z zastosowaniem perforacji żeber**

Wing is cut by an undeformable cylinder in LS-Dyna (Morka et al. 2013)

W1: 2mm otw. **μ=0,5** EPS=0,1	**W2: 2mm otw. μ=0,5** EPS=0,2
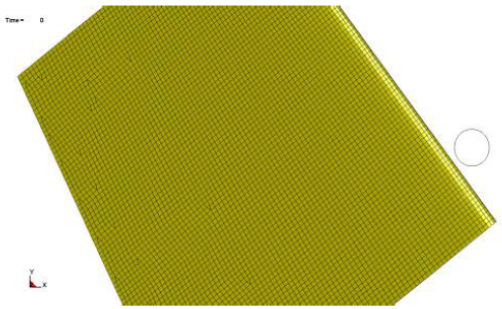	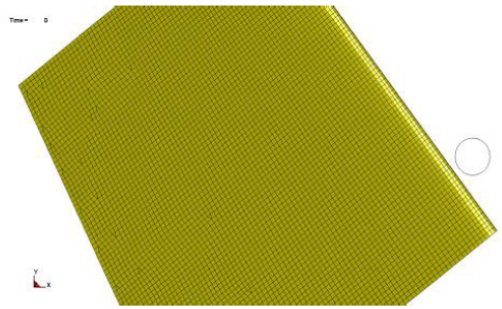
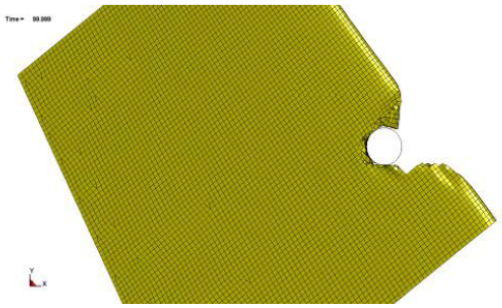	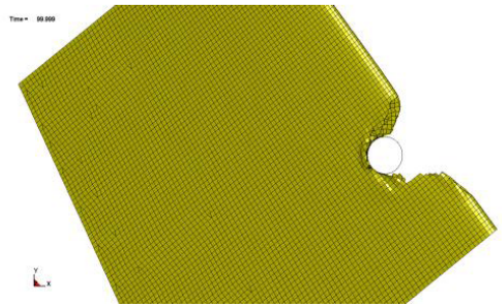
	

Cutting the wing in LS-Dyna (Morka et al. 2013)

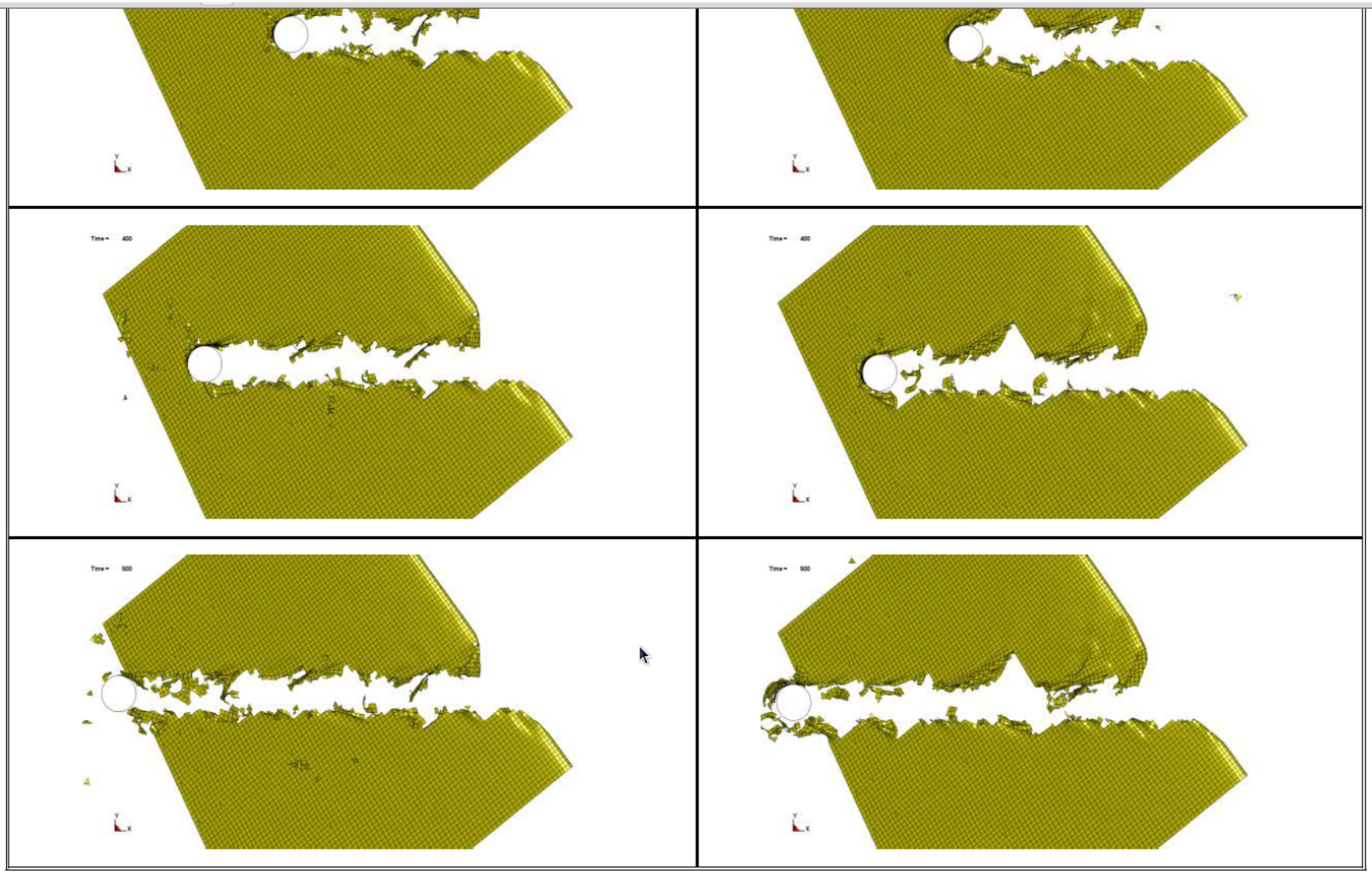

Rys. 9. **Deformacja i niszczenie skrzydła dla dwóch wielkości zastępczego odkształcenia niszczącego w kolejnych chwilach czasu.**

Tab. 6. **Wyniki testów wariantowych dla różnych wartości parametrów**

force aver. force

simlation parameters, thickness of metal sheets etc.	**Siła** maksymalna [kN]	**Siła średnia** [kN]
1mm μ=0,5 EPS=0,1	163	79,3
2mm μ=0,5 EPS=0,1	374,3	172,1
3mm μ=0,5 EPS=0,1	611,9	248,1
1mm otw. μ=0,5 EPS=0,1	161,5	77,3
2mm otw. μ=0,5 EPS=0,1	329,8	149,9
3mm otw. μ=0,5 EPS=0,1	534,3	231,2
2mm otw. μ=0,5 EPS=0,2	797,1	407,3
2mm otw. μ=0,1 EPS=0,1	435,4	164,8
1mm gęsty μ=0,5 EPS=0,1	144,8	54,2
2mm gęsty μ=0,5 EPS=0,1	274,6	127,2
3mm gęsty μ=0,5 EPS=0,1	418,3	190,4
1mm otw.gęsty μ=0,5 EPS=0,1	121,7	49,8
2mm otw. gęsty μ=0,5 EPS=0,1	212,6	99,5
3mm otw. gęsty μ=0,5 EPS=0,1	362,9	163,9

Force as a function of displacement, for different mean aluminum alloy thicknesses

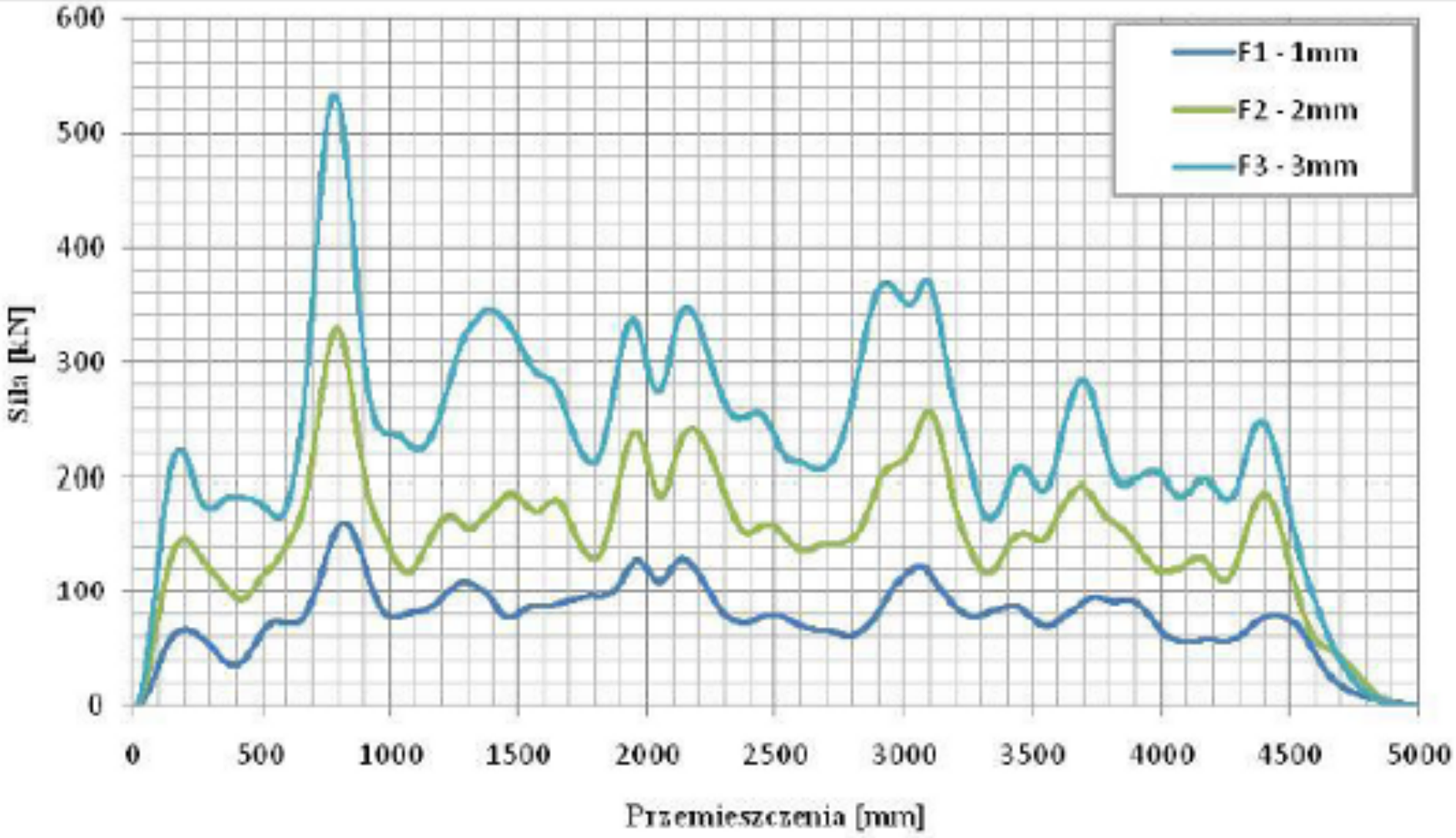

How max. deformation parameters influence the wing-tree force.

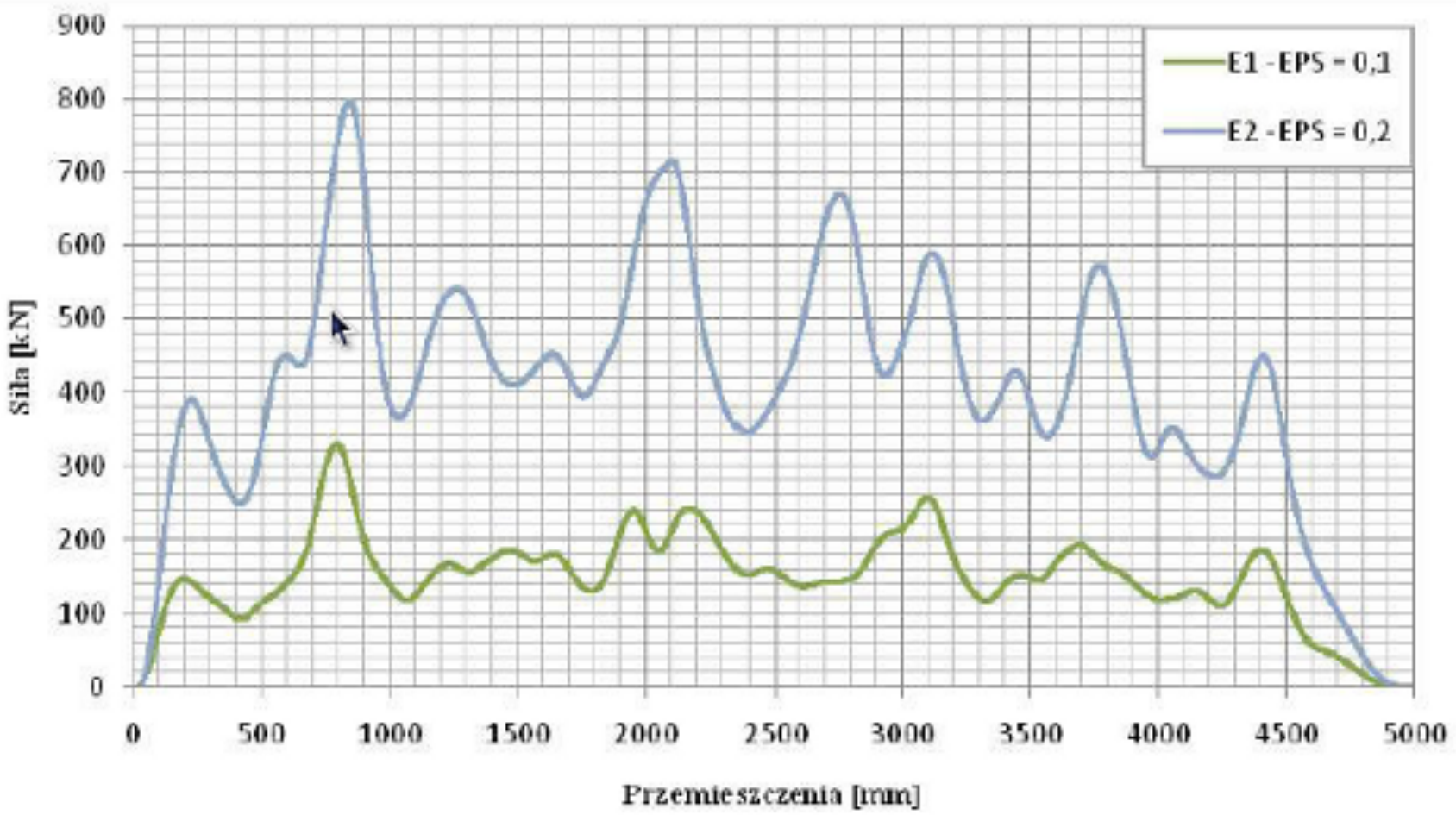

Influence of the resultion of the mesh (green is sparse grid, blue is dense grid)

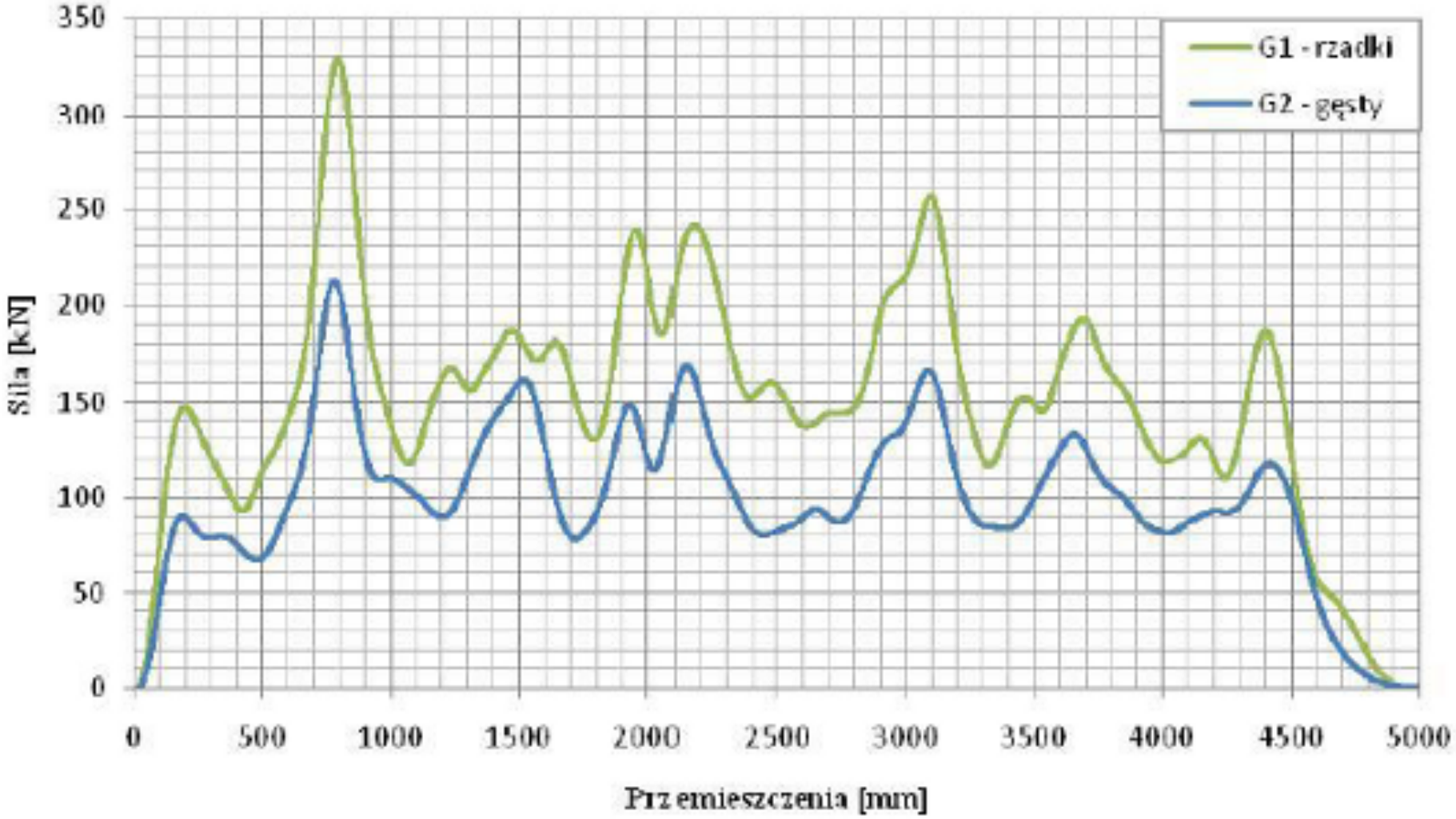

CALCULATIONS OF TREE BREAKING

- Essential variable: the total force of tree-wing contact
- Realistic force in higer-resolution FEM equals 20-30 tonnes
- I will show the tree deformation calculations done in the IDL language
- Mathematical model: Timoshenko beam =
- Euler-Bernoulli beam generalized to include shear deformations and rotational inertia
- I further generalized that model to include axial strains and stresses, and a more tree-like, variable cross section

Generalized TIMOSHENKO BEAM

$$m\frac{\partial^2 w}{\partial t^2} + \eta(x)\,\frac{\partial w}{\partial t} = \frac{\partial}{\partial x}\left[\kappa AG\left(\frac{\partial w}{\partial x} - \varphi\right)\right] + q(x,t)$$

$$J\frac{\partial^2 \varphi}{\partial t^2} = N\frac{\partial w}{\partial x} + \frac{\partial}{\partial x}\left(EI\frac{\partial \varphi}{\partial x}\right) + \kappa AG\left(\frac{\partial w}{\partial x} - \varphi\right)$$

Model allows to study the deformations of elastic columns or beams subject to bending and shear, as well as additional axial loading such as the gravity of the beam. The above equations have been supplemented by axial mtion equation, to take into account vertical component of deformation in a dynamic setting. The tree has a circular cross section and narrows from bottom to top.

Time-variability of force (cf. Morka 2013) with the average 22 T and 32 T of force

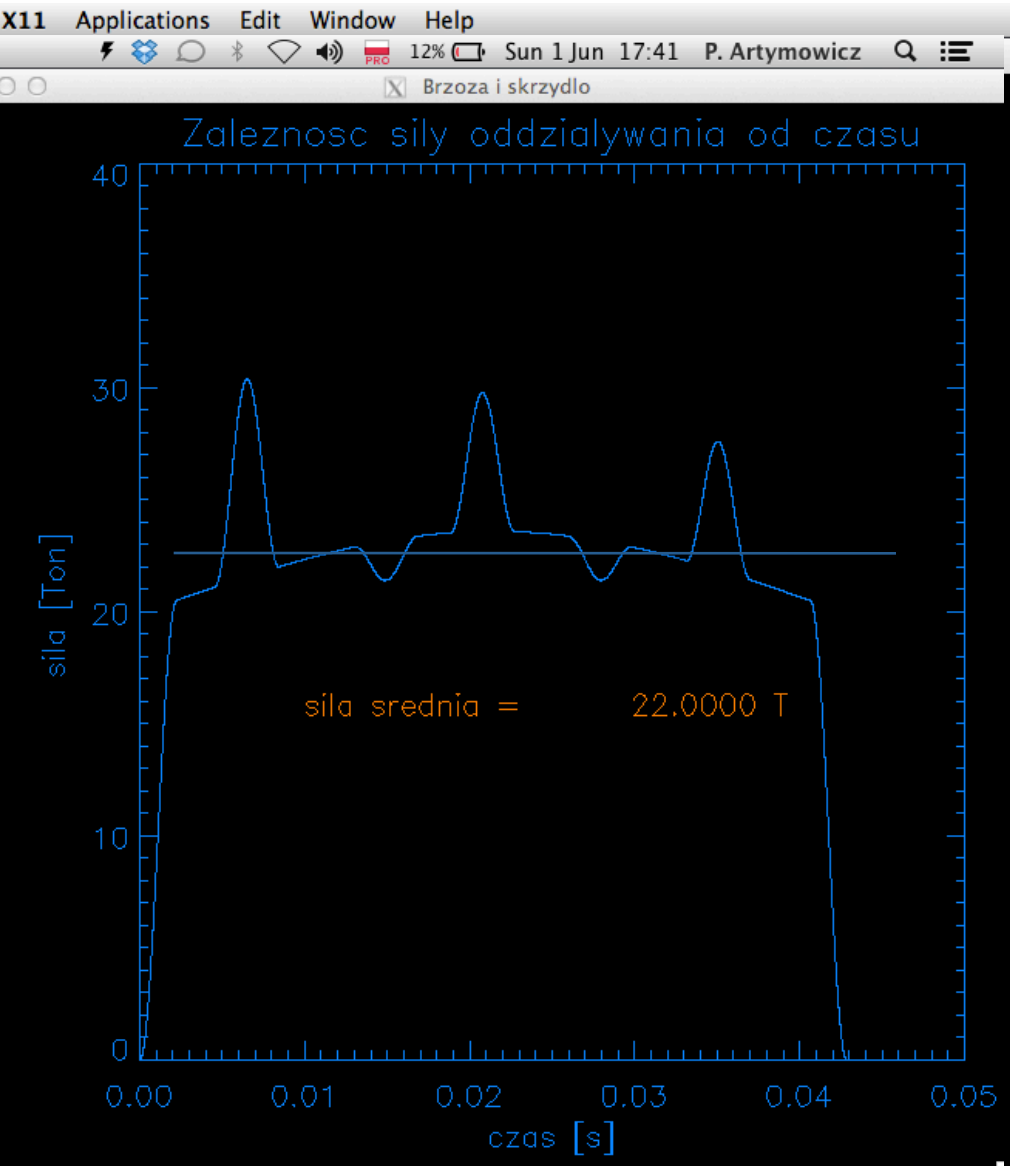

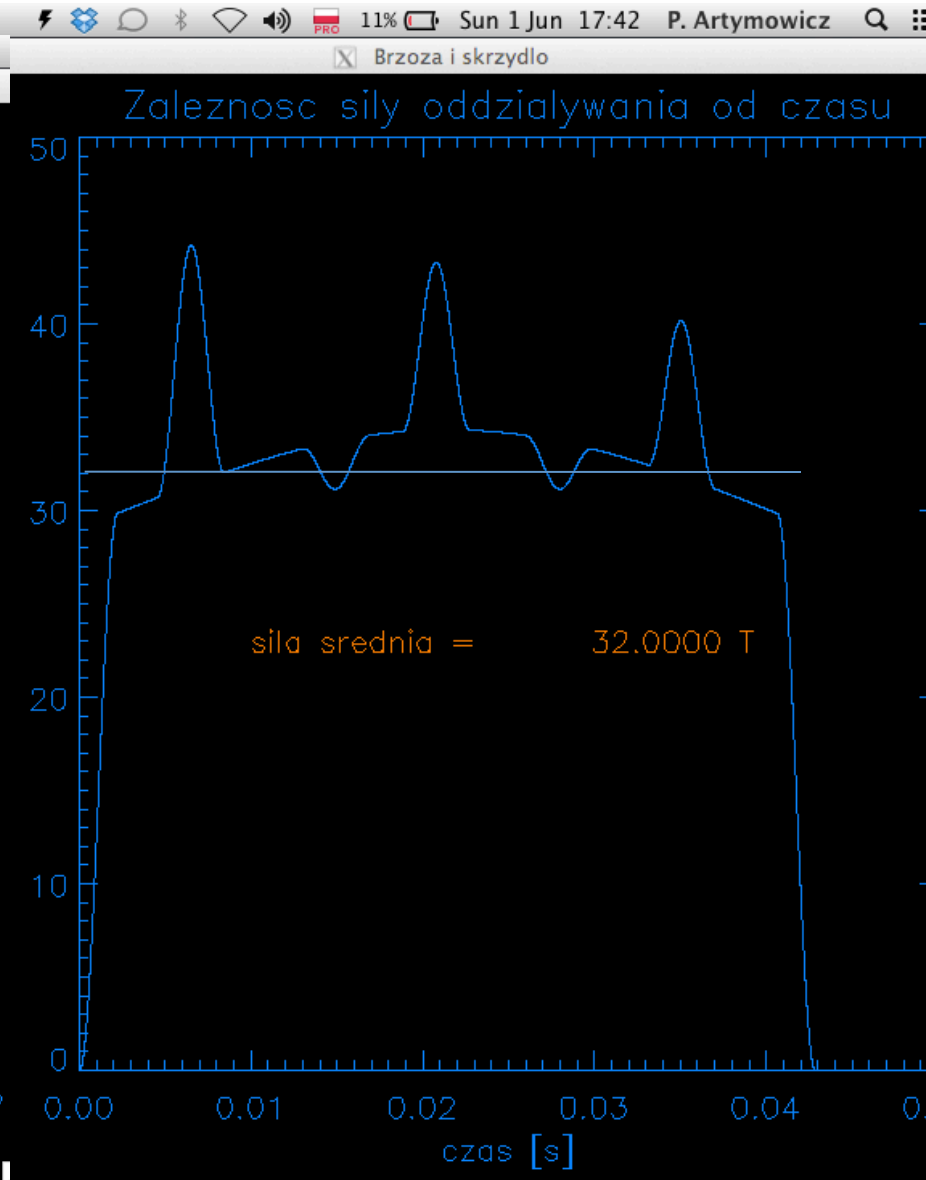

Force 22 T, t = 9 ms,

Map of absolute (left) and relative (right) axial stress on fibers

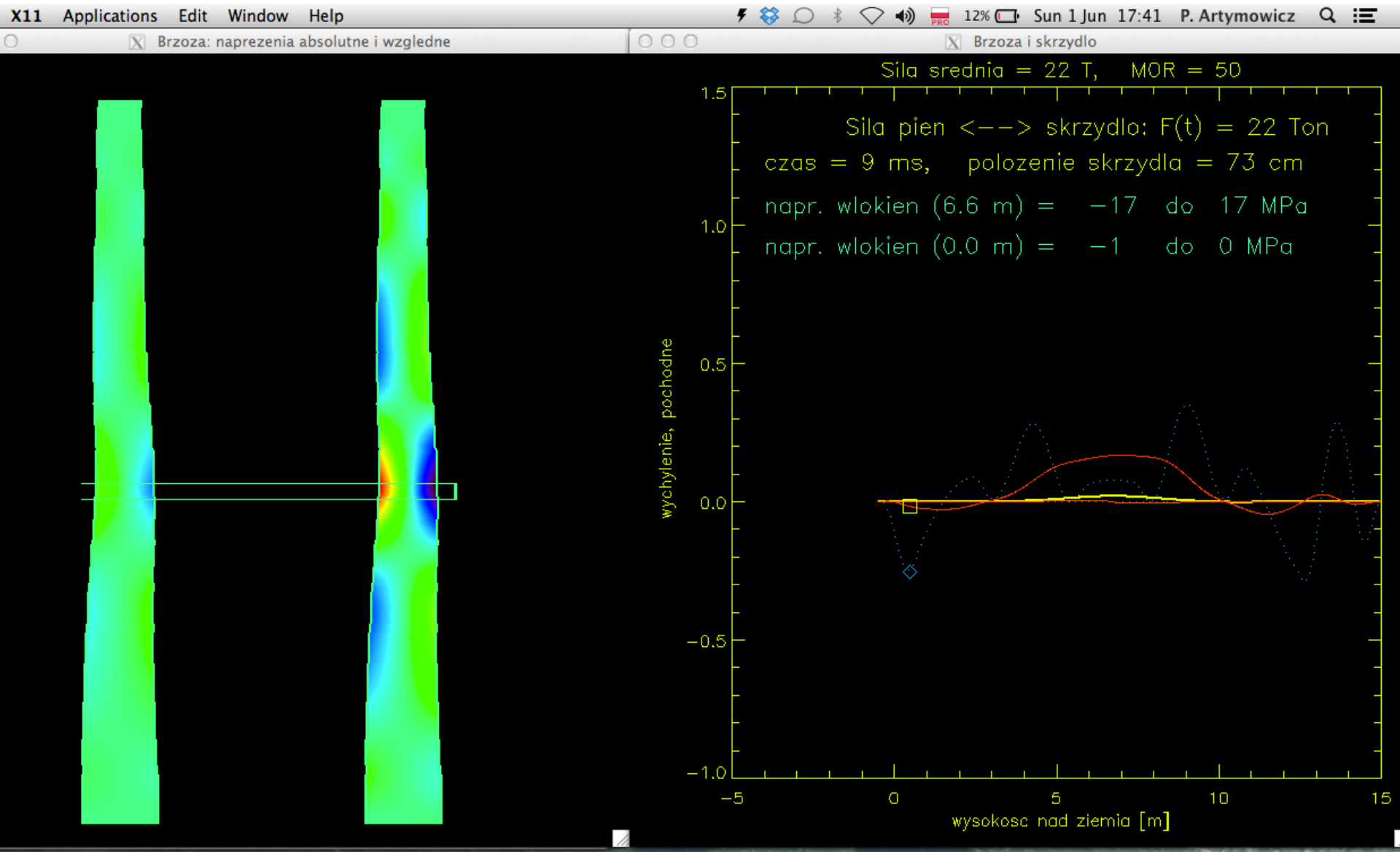

Force 22 T, time t = 39 ms, stresses at 6.5m height = (+-42) in MPa. In this case there is no breakage; the trunk deflects by up to ~0.2 m

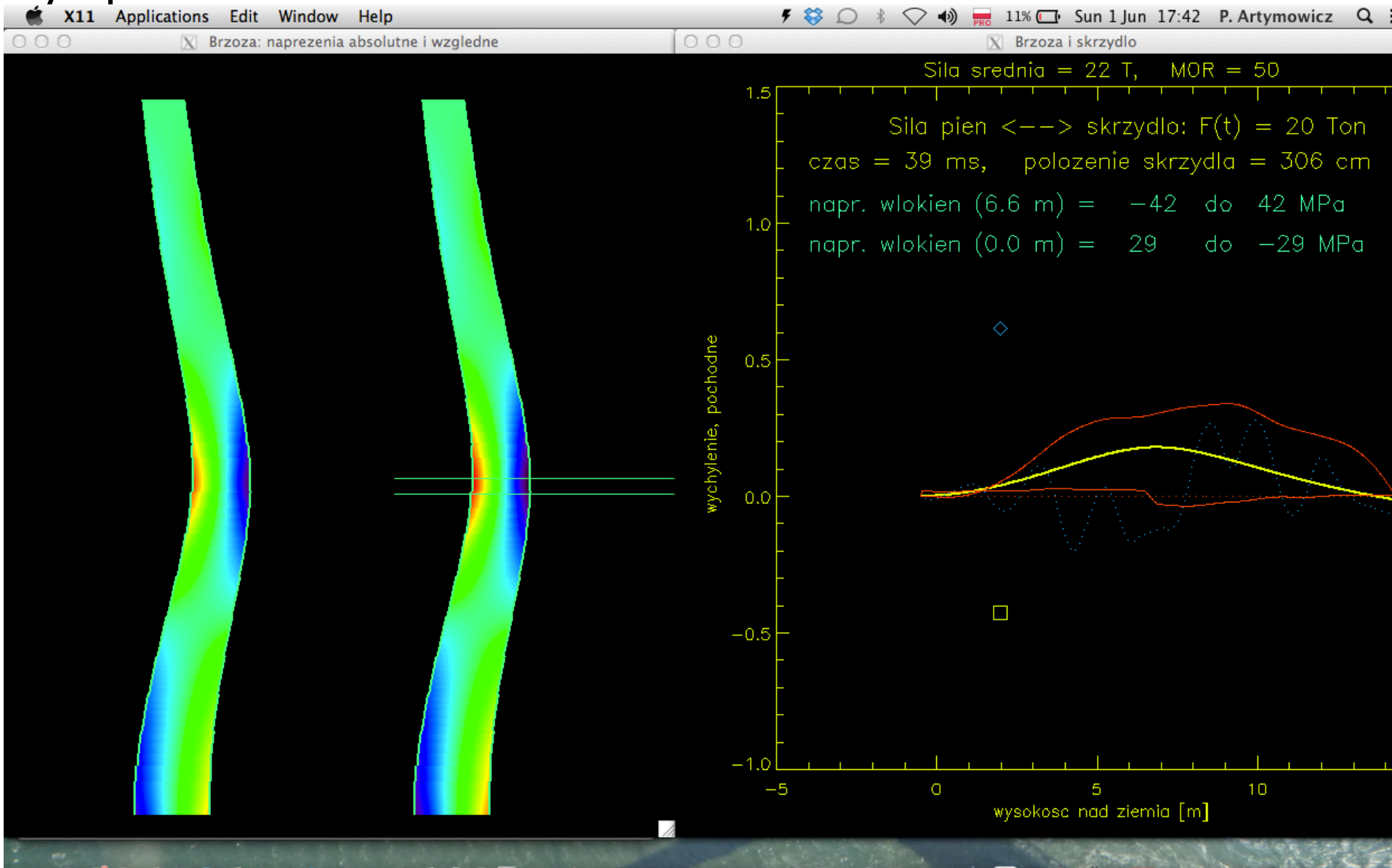

Force 27 T, time t = 9 ms

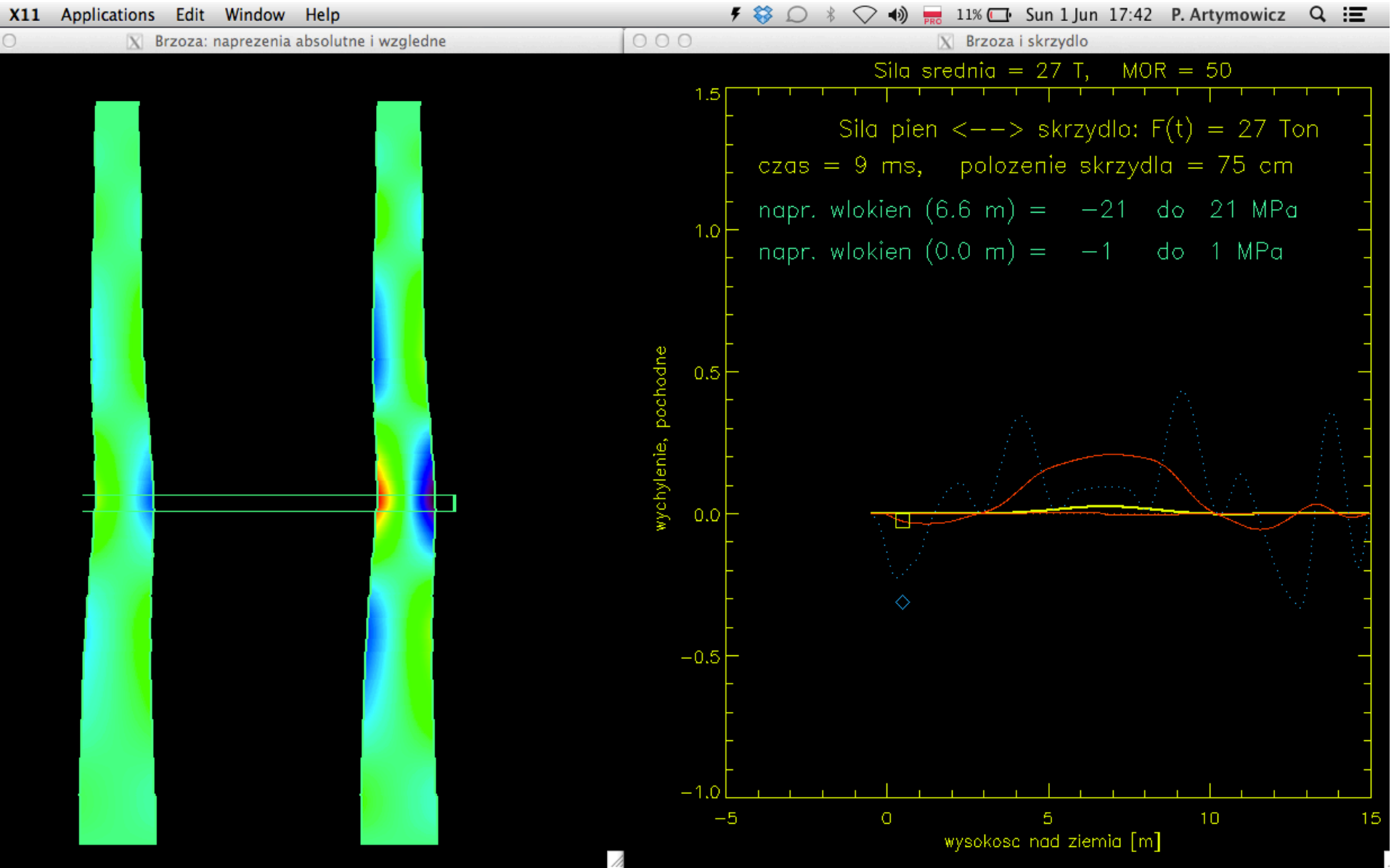

Force 27 T, time t = 23 ms

Tension of fibers exceeds at the height of 6.5 m, as well as 0.6 m the limiting values (moduls of rupture for birch MOR ~ 50 MPa).

A wavetrain of shear and dilatation waves is launch travels along the tree trunk.

(The fracture is not of a splinter type because of the low dimensionality of the Timoshenko beam model)

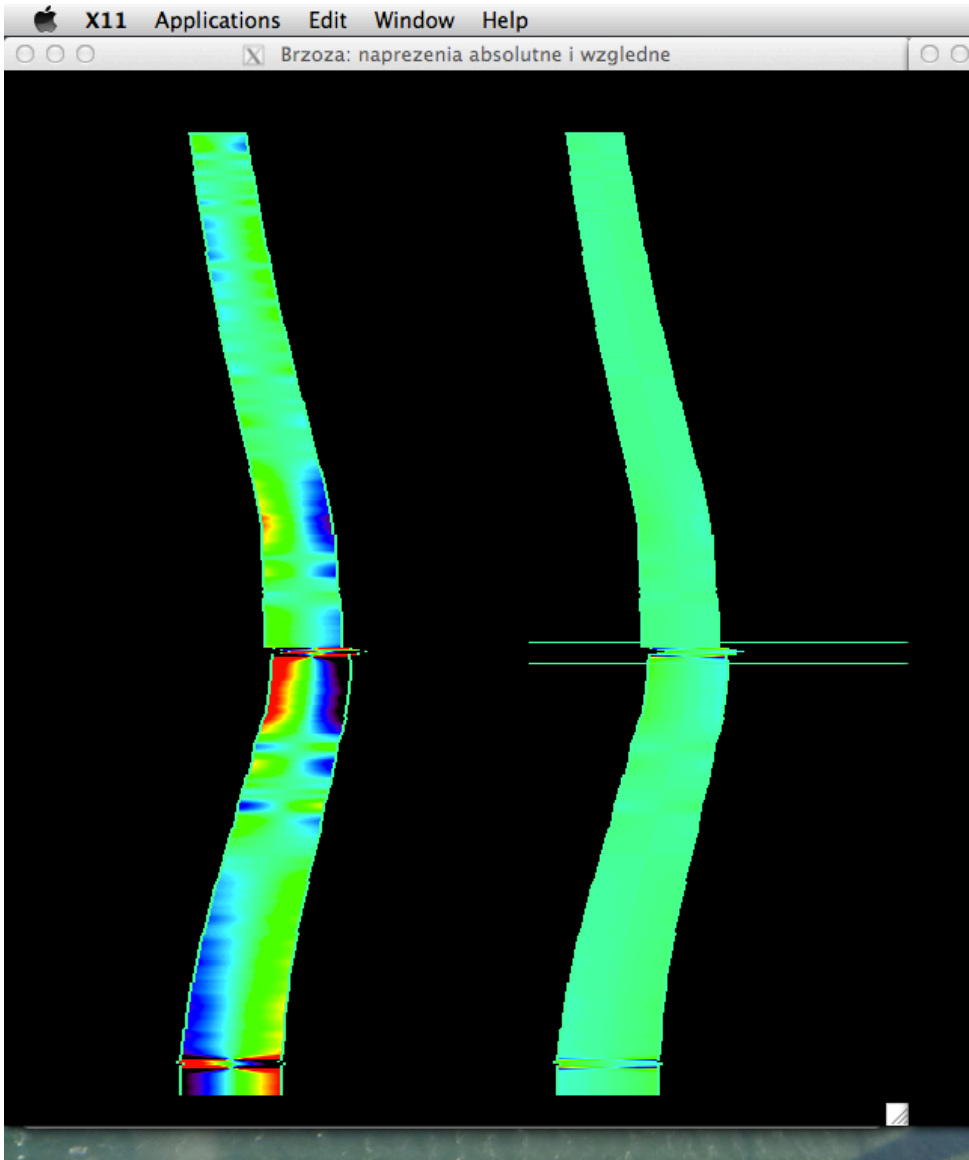

Results

The tree trunk of the Bodin's birch modeled under realistically time-variable loading (the variability patterned after FEM calculations of Morka et al. 2012) with a mean force of 22 tonnes does not cause the breakage of the trunk

- Mean contact force of ~26 tonnes or larger causes fractures in the trunk (MOR is locally exceeded). The trunk is broken in two areas: one in the area hit by the wing and the other at the base near the ground, exactly as it happened in Smolensk in 2010. Mean force > ~30 ton (300 kN) requires too thick aluminum alloy sheets in the wing to be generated.
- The current model has reduced dimensionality and cannot answer all question, e.g. what is the deviation of the line of breakage of the wing from the direction of flight, what is the shape of fractures. Realistically they would have long splinters. More calculations are needed, although it seems concievable that that the trunk hit by the delta-shaped wing, by deflects by the right amount to explain the small tilt of the cut line to the flightpath.

Results

- In first approximation, an FEM simulation of the structure of the wing under collision with a tree can be done with a nondeformable obstacle, because the wing structural failure happens rapidly, in time when a large tree inertia excludes its rapid deformation. Such method was employed by the WAT research group of Morka et al.
- If however we want to reproduce the slightly slanted cut line of the wing (8 degrees w.r.t. flight direction) then we'd need to use a deformable trunk such as the one studied here, maybe also the small, planar wing distortion along its whole span. The task seems easy, since our ~0.5 m bending corresponds to exactly such a slant angle given a ~3.5 meter long chord of the wing.

Results

- Destruction of a box structure of the wing always happens in correctly performed simulations
- Metal sheet thickness of order 2-3 mm leads to just enough loading on a 44 cm-diameter tree to cause its breakage. This happens long after the fate of the wing is already sealed: the breakage occurs when the wing is already largely cut off and it is leaving the area of interaction in two pieces.

Executive Summary:
(i) the problem of flight of the detached wingtip of the Smolensk Tupolev PLF 101, and
(ii) the problem of the wing-tree collision
have been solved.

- Theoretical flight path of the 6.5-m part of the left wing agrees very well with the distance from the Bodin's birch tree to the place whe it fell (110 m), and its very well-preserved state.
- The calculated, complex, tree breakage (at two different heights in the opposite directions) long after the initiation of wing destruction (under the mutual force of about 27-30 tonnes), is in a good agreement with the post-accident reports of Smolensk crash.